AD-A179 466 MONOLITHIC THIN FILM SAW (SURFACE ACOUSTIC WAVE) DEVICES IMPLANT-ISOLATED (U) PURDUE UNIV LAFAYETTE IN SCHOOL OF ELECTRICAL ENGINEERING R L GUNSHOR ET AL 1/1

UNCLASSIFIED 01 SEP 85 AFOSR-TR-87-0496 AFOSR-83-0237 F/G 9/5 NL

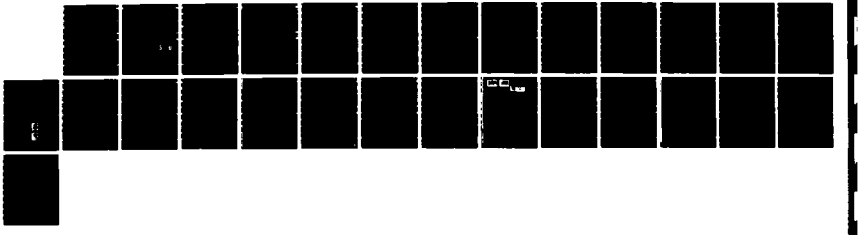

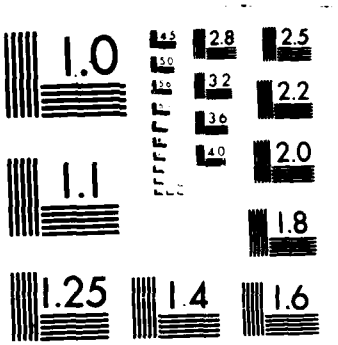

(2)

UNCLASSIFIED

SECURITY CLASSIFICATION OF THIS PAGE (When Data Entered)

REPORT DOCUMENTATION PAGE		READ INSTRUCTIONS BEFORE COMPLETING FORM
1. REPORT NUMBER AFOSR-TR- 87-0496	2. GOVT ACCESSION NO.	3. RECIPIENT'S CATALOG NUMBER DTIC FILE COPY
4. TITLE (and Subtitle) Monolithic Thin Film SAW ~~Structures~~ DEVICES Implant-Isolated Surface Storage Correlator		5. TYPE OF REPORT & PERIOD COVERED Interim Scientific Report 1 July 84 to 31 August 85
		6. PERFORMING ORG. REPORT NUMBER
7. AUTHOR(s) R. L. Gunshor, S. Datta, and N. Otsuka*		8. CONTRACT OR GRANT NUMBER(s) AFOSR-83-0237
9. PERFORMING ORGANIZATION NAME AND ADDRESS School of Electrical Engineering (*School of Purdue University Materials Eng) West Lafayette, IN 47907		10. PROGRAM ELEMENT, PROJECT, TASK AREA & WORK UNIT NUMBERS 2306/B2
11. CONTROLLING OFFICE NAME AND ADDRESS Air Force Office of Scientific Research Building 410 Bolling AFB, D.C. 20332 NE		12. REPORT DATE 1 September 1985
		13. NUMBER OF PAGES
14. MONITORING AGENCY NAME & ADDRESS(if different from Controlling Office) SAME		15. SECURITY CLASS. (of this report) UNCLASSIFIED
		15a. DECLASSIFICATION/DOWNGRADING SCHEDULE

16. DISTRIBUTION STATEMENT (of this Report)
Approved for public release; distribution unlimited.

17. DISTRIBUTION STATEMENT (of the abstract entered in Block 20, if different from Report)
SAME

DTIC ELECTE APR 2 3 1987 S D

18. SUPPLEMENTARY NOTES
N/A/

19. KEY WORDS (Continue on reverse side if necessary and identify by block number)
Surface acoustic waves; ZnO, storage correlators; resonators; X-ray sources; Molecular Beam Epitaxy; II-VI Semiconductors, Multiple Quantum Wells, Superlattices.

20. ABSTRACT (Continue on reverse side if necessary and identify by block number)
A new surface acoustic wave resonator provides for greatly relaxed fabricational tolerances. The first multiple quantum well and superlattice structures are reported for the wide bandgap semiconductor system (Zn,Mn)Se.

[illegible] 16-4-1931 NE

DD FORM 1 JAN 73 1473 EDITION OF 1 NOV 65 IS OBSOLETE

87 4

SECURITY CLASSIFICATION OF THIS PAGE (When Data Entered)

RESEARCH OBJECTIVES

Introduction

The Research reviewed in this report reflects the fact that the period reviewed was one of transition between the past emphasis on monolithic (ZnO-on-silicon) surface acoustic wave devices, to the present activity focused on the development of new device concepts based on the use of II-VI semiconductor materials in configurations fabricated using molecular beam epitaxy (MBE). The new emphasis is on the wide gap II-VI semiconductors, and includes the growth and evaluation of superlattice and quantum well structures in the $ZnSe/Zn_{1-x}Mn_xSe$ materials system.

Specific Results

A. Implant-Isolated Storage Correlator

The past year saw the completion of our work on monolithic devices used to perform real-time nonlinear signal processing in the VHF/UHF portion of the rf spectrum. Details of the fabrication and operating characteristics of this particular device, together with a brief review of the progress of the field, were included in an invited paper for a special issue of the IEEE Transactions on Sonics and Ultrasonics devoted to surface acoustic wave convolvers and correlators (Appendix A).

B. Mode Conversion Resonators

A new surface acoustic wave resonator configuration was developed which has the advantage of eliminating the critical positioning requirement for the input/output interdigital transducers, a characteristic feature of conventional SAW resonators. The key factor leading to this advantage is the resonator concept (developed under AFOSR support) utilizing Rayleigh-Sezawa mode conversion. In this concept the reflectors are replaced by periodic gratings which provide for a conversion between the Rayleigh and Sezawa wave models. This appears to be a novel concept, as we know of no other instance where a mode conversion, occurring with such high efficiency, is employed to implement a useful device function. Details of these resonators are found in the publication reprinted in Appendix B.

C. Novel Applications of Multilayered Structures and Superlattices

During this period three ideas for novel applications of ultrathin layered structures were pursued theoretically, though no experimental work was done due to practical limitations. First, we considered the possibility of a new kind of space charge wave in a pair of quantum wells that could be useful for signal processing in the infrared. Second, we discussed the possibility of generation of visible and UV

radiation by electron beams traversing a superlattice. This work has been pursued further by one of our colleagues (A. E. Kaplan). Third, we explored the possibility of new guided acoustic waves in layered structures that could lead to the development of integrated acoustics similar to integrated optics.

D. Molecular Beam Epitaxy of Wide-gap II-VI Semiconductors

During the past year, considerable progress was made in developing techniques for the fabrication of superlattice and quantum well structures based on ZnSe. Having a direct bandgap in the blue portion of the visible spectrum, structures based on ZnSe hold promise for new light emitting devices. Quantum well structures were formed using the bandgap modulation provided by incorporation of Mn (substituting on Zn sites) into ZnSe. By means of collaborations with several other groups, a wide range of techniques were used for the evaluation of the (Zn,Mn)Se structures. During the reporting period, two publications were prepared which describe the growth, microstructural evaluation, and optical properties of these structures. (Appendix C and D).

PUBLICATIONS

S. W. Schwartz, R. L. Gunshor, and R. F. Pierret, "Implant-Isolated SAW Storage Correlator," INVITED, IEEE Transactions on Sonics and Ultrasonics (Special Issue on SAW Convolvers and Correlators SU–32, 707 (1985).

S. S. Schwartz, S. J. Martin, R. L. Gunshor, S. Datta, and R. F. Pierret, "SAW Resonators Insensitive to IDT Position," Proceedings 1984 IEEE Ultrasonics Symposium, p. 229 (1984).

A. E. Kaplan and S. Datta, "Extreme-Ultraviolet and X-ray emission and amplification by nonrelativistic electron beams traversing a superlattice," Appl. Phys. Lett. 44, 661 (1984).

L. A. Kolodziejski, R. L. Gunshor, T. C. Bonsett, R. Venkatasubramanian, S. Datta, R. B. Bylsma, and W. M. Becker, "Wide Gap II-VI Superlattices of ZnSe-ZnMnSe, Appl. Phys. Lett. 47, 169 (1985).

Y. Hefetz, J. Nakahara, N. V. Nurmikko, L. A. Kolodziejski, R. L. Gunshor, and S. Datta, "Optical Properties of ZnSe/(Zn,Mn)Se Multiquantum Wells," Appl. Phys. Lett. 47, 989 (1985).

R. L. Gunshor, N. Otsuka, M. Yamanishi, L. A. Kolodziejski, T. C. Bonsett, R. B. Bylsma, S. Datta, "Diluted Magnetic Semiconductor Superlattices," Invited paper presented at 2nd International Conference on II-VI Compounds, Aussois (France), March 1985.

PERSONNEL

Robert L. Gunshor, Professor of Electrical Engineering
Supriyo Datta, Associate Professor of Electrical Engineering
Nobuo Otsuka, Assistant Professor of Materials Engineering
Stephen S. Schwartz, Graduate Research Assistant
Biswajit Das, Graduate Research Assistant
Timothy J. Miller, Technician

DEGREES AWARDED

Stephen S. Schwartz, Ph.D., "Zinc Oxide-on-silicon Surface Acoustic Wave Devices," May 1985.

IEEE TRANSACTIONS ON SONICS AND ULTRASONICS, VOL. SU-32, NO. 5, SEPTEMBER 1985

Implant-Isolated SAW Storage Correlator

STEPHEN S. SCHWARTZ, ROBERT L. GUNSHOR, SENIOR MEMBER, IEEE, AND ROBERT F. PIERRET, SENIOR MEMBER, IEEE

Abstract—The development of surface acoustic wave (SAW) convolvers and correlators is reviewed. This is followed by the introduction of a new type of monolithic metal-zinc oxide-silicon dioxide-silicon storage correlator. Fabrication and operation of the implant isolated storage correlator, which relies on ion implantation for confinement of storage regions, is detailed. A capacitance-time measurement procedure for evaluation of the charge storage capability of the device is described, and correlation output information is used to estimate the effective recombination rate of the inversion layer charges. Finally, operational characteristics are examined and the new bias stable device is shown to exhibit a 3-dB storage time in excess of 0.5 s. The cited storage time exceeds reported storage times of other structures fabricated in the ZnO-SiO_2-Si layered medium configuration.

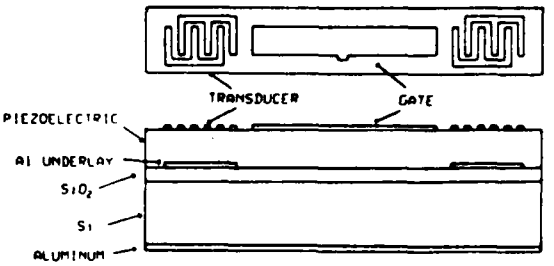

Fig. 1. Schematic of a typical monolithic SAW correlator.

I. Introduction

SURFACE acoustic wave (SAW) convolvers and memory correlators are devices that utilize the nonlinear interaction of the electric field associated with acoustic waves in a piezoelectric medium to perform real time multiplication of two signals. A representative monolithic metal-piezoelectric film-SiO_2-Si convolver is shown in Fig. 1. The piezoelectric layer enables one to excite surface acoustic waves in the silicon by applying RF signals to interdigitated transducers on the surface of the substrate. The electric field pattern produced by fingers of alternating polarity induce periodic time and spatial stresses in the piezoelectric layer, thereby exciting a surface acoustic wave. Associated with each propagating surface wave is an accompanying electric field. It is the nonlinear interaction within the semiconductor between the electric field patterns of two contra-propagating waves that produces a signal proportional to the product of the two acoustic signals at every point in the device. The function of the third electrode, known as the gate, is to sum the product signal over the length of the device. When two signals are applied simultaneously to the two transducers, the output at the gate is proportional to the time-compressed convolution of the two signals.

The family of monolithic SAW devices includes structures fabricated on GaAs substrates, which have demonstrated outstanding time-bandwidth products [1]. Because of the relatively weak piezoelectric nature of the GaAs, however, these devices, when implemented without a piezoelectric film overlayer, have lower correlation efficiencies at wide bandwidth compared to other configurations—even though substantial progress has been made toward improving these efficiencies [2]. The development of layered medium monolithic SAW devices has emphasized the use of ZnO and AlN as piezoelectric films. Although ZnO was the first thin film having high performance in the SAW context [3], and hence has received the most attention [4], [5], AlN [6]-[8] has some attractive features related to ruggedness and the potential for low dispersion. Both materials can be utilized to achieve a temperature stable configuration.

It should be noted that the configuration of Fig. 1 is but one of several ways to realize the piezoelectric-semiconductor interaction. For example, a separated-medium technique has been employed where a semiconductor (Si) and a bulk piezoelectric crystal (usually $LiNbO_3$) are mounted in close proximity [9]-[14]. The separated medium structure, although mechanically more complex than a monolithic configuration, has a wide bandwidth capability [15] as a result of the high electromechanical coupling coefficient of $LiNbO_3$. To increase the bandwidth capability of devices fabricated in the monolithic ZnO-SiO_2-Si system—thereby making them more attractive as practical signal processing devices—higher electromechanical coupling was sought by employing a higher order Rayleigh mode. It has been shown that the second-order or Sezawa mode of the layered ZnO-SiO_2-Si configuration can be efficiently excited in high-quality films [16]. The electromechanical coupling coefficient available from this mode exceeds that for Rayleigh waves in bulk ZnO, and is close to the value for $LiNbO_3$. Several convolvers and diode storage correlators which exploit the bandwidth advantage of the Sezawa mode have been reported [17]-[20].

Convolvers, it should be pointed out, can be used to perform correlation between two signals. A disadvantage of correlating two signals using a convolver is that the ref-

Manuscript received September 1, 1984; revised January 22, 1985. This work was supported by the Air Force Office of Scientific Research under Grant AFOSR-83-0237.

The authors are with the School of Electrical Engineering, Purdue University, West Lafayette, IN 47907, USA.

0018-9537/85/0900-0707$01.00 © 1985 IEEE

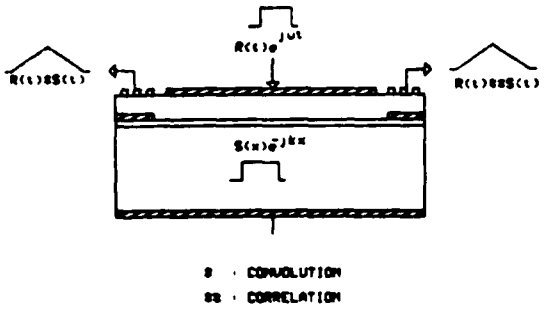

Fig. 2. Correlation and convolution using a storage correlator.

erence signal must be time reversed. An electronic time-reversal technique [21] has been demonstrated in a convolver system [22], but at a sacrifice of high insertion loss which leads to a degraded dynamic range. Additionally, an incoming signal arriving at an unknown time necessitates repeated application of the reference signal to counter the uncertainty of the arrival time which in turn leads to a smaller effective time-bandwidth product.

The storage correlator is a device that performs both convolution and correlation without the need for time reversal and without concern for the uncertainty of the arrival time of the signal to be interrogated. Hence, two of the major drawbacks of performing correlation with the convolver system are eliminated by utilizing a memory correlator.

A simplified description of the storage correlation process can be given with the aid of Fig. 2, which depicts a typical memory correlator. Under normal operation, one introduces a signal at one of the transducers such that a sampled version of this reference signal $S(t)$ is stored beneath the gate of the device by one of several possible writing procedures. At some later instant, but still within the storage time of the reference signal, a second signal $R(t)$ is applied to the gate of the correlator. The introduction of $R(t)$ at the gate electrode excites two contra-propagating signals representing the product of $R(t)$ and $S(t)$, which subsequently appear at the two output transducers; it can be shown that the correlation appears at one transducer, while the convolution output is available at the other.

To date, several memory-array configurations have been employed in the fabrication of storage correlators. Schemes for signal storage by means of surface states [23], [24], p-n diodes [18], [25]-[28], and Schottky diodes [29]-[31] have been examined. More recently, a new type of junction storage correlator has been introduced [32], in which the spatial variation of inversion layer charge at the SiO_2-Si interface of the ZnO monolithic configuration has been utilized for signal storage. With the exception of this "induced junction" storage correlator, the various storage schemes have been employed in both monolithic and separated medium configurations.

The first memory devices utilized semiconductor surface states for signal storage [23], [24]. In a surface state memory correlator, the electric field pattern associated with an applied signal causes a bunching (periodic spatial concentration) of free electrons at the Si-SiO_2 interface. Subsequently, a portion of the electrons are trapped at the interface thereby producing a spatially varying charge pattern. The storage time of these devices corresponds to the detrapping time, which is a function of the properties of the interface. Surface state storage was subsequently replaced by more easily controlled and repeatable diode storage arrays. More recently, reference-signal storage in induced junctions was reported [32]. In both diode and induced junction-array processes, the principle of charge storage is essentially the same. Recombination of minority carriers injected out of a p^+ region (or inversion layer in the case of the induced junction device) by an applied signal causes an alteration of the diode (induced junction) depletion width.

The monolithic metal-ZnO-SiO_2-Si (MZOS) [33], [34] memory correlator introduced in this paper utilizes depletion regions in the silicon to store a reference signal, but in a metal-oxide semiconductor (MOS) region of n-type silicon only; that is, no diodes or surface states are employed for storage. Furthermore, the uncontrollable and often undesirable charge-injection process [31], [35]-[37] which was used constructively by the induced junction storage correlator is successfully ignored in the implant-isolated storage device.

In the following section we present a detailed description of the implant-isolated storage correlator fabrication and operation as well as experimental verification of the existence of induced junction storage regions. Section III consists of an in-depth discussion of charge storage in the implant-isolated device. An approximation for the effective recombination lifetime of minority carriers is also presented. Experimental results for the implant-isolated storage correlator are given in Section IV followed by conclusions in Section V.

II. The Implant-Isolated Structure

Device Structure

The implant isolated storage correlator, pictured in Fig. 3, consists of an n-type 10-Ω-cm (100)-cut silicon substrate, which is ion implanted with phosphorus in a grating pattern at the sample surface. Charge storage, it should be noted, occurs in the nonimplanted regions. Subsequent to the grating region implantation, a wet oxidation is performed at 900°C for 40 min. This oxidation, yielding a 1000-Å-thick insulating layer, simultaneously passivates the silicon surface and activates the implant. Prior to depositing the 1.7-μm ZnO layer by RF sputtering, 1000-Å-thick aluminum shorting planes are evaporated on the substrate in the regions below the transducers to enhance the electromechanical coupling. The top aluminum metallization pattern consists of two pairs of single comb transducers [38] and a split gate electrode arranged so as to form a dual-track structure [39]. The transducers, used to excite Rayleigh waves, have equal 17.75-μm finger widths and gaps; the center frequency of the transducer response is 128 MHz. The separate comb dual-track structure is employed because this technique has been shown to sup-

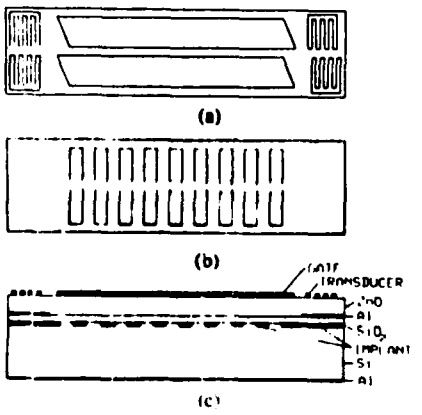

Fig. 3. Schematic diagram of an implant-isolated storage correlator. (a) Top view of dual-gate structure and single-comb transducers. (b) Ion implantation pattern. (c) Side view of completed device.

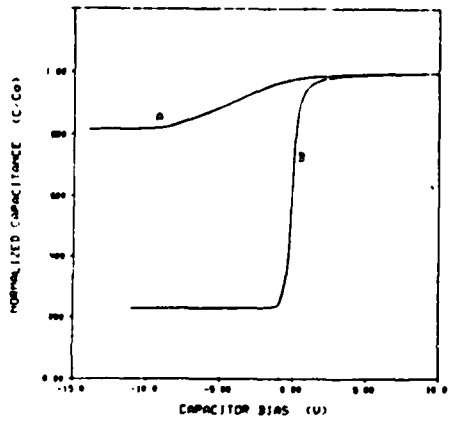

Fig. 4. Normalized C–V curves for typical MOS capacitors. *A* and *B* denote the highly doped ($1.25 \times 10^{17}/cm^3$) n-type Si and moderately doped ($5.0 \times 10^{14}/cm^3$) n-type Si, respectively.

press the self-convolution caused by reflections from the transducers. By slanting the gate metallization pattern adjacent to the transducers one minimizes the undesirable output observed at the transducers caused by waves launched at the ends of the gate.

Concept of Implant-Isolation

Insight into the operation of the implant-isolated storage correlator can best be achieved by understanding the method in which charge is stored in the device. We present a qualitative explanation based on typical n-type MOS capacitance versus voltage characteristics. To first order the ZnO layer can be modeled as a constant capacitance in series with the constant SiO_2 layer capacitance; the combination can in turn be modeled as a single effective insulating layer. The C–V curves for two structurally identical but differently doped metal-insulator-semiconductor (MIS) capacitors are displayed in Fig. 4. Note that for both devices, accumulation occurs over the same bias range. However, the onset of inversion occurs for different values of capacitor bias. Suppose the two differently doped devices were side-by-side as part of the same substrate and covered by the same insulator and metal gate. Under this

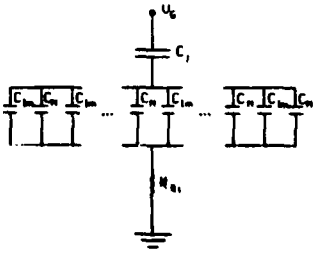

Fig. 5. Electrical model for the gate of the implant-isolated storage correlator. The implanted and nonimplanted regions are denoted by C_{Im} and C_N respectively. R_{Si} is the bulk silicon resistance and C_i is the combined oxide capacitance.

condition a range of gate bias voltage would exist where the higher doped device would be depleted and the lower doped device would be inverted. In the implementation of the implant-isolated storage correlator, higher doped depletion regions are used to isolate the lower doped storage or inversion regions.

To achieve lateral variations in doping density one can employ either ion implantation or diffusion; ion implantation was chosen because it offered advantages in ease of fabrication. Phosphorus was implanted into the unoxidized silicon wafer through a photoresist mask at a concentration level of $8.0 \times 10^{12}/cm^2$ using an implant energy of 25 keV. The implant concentration varies of course as a function of depth into the semiconductor. An estimate of the doping profile derived from the C–V profiling technique, however, indicates that the semiconductor may be approximately modeled as uniformly doped ($\sim 10^{17}/cm^3$) in the bias range of interest. As a result of the ion implantation, a periodic grating pattern of alternating highly doped and lowly doped semiconductor is established beneath the gate of the correlator. The periodicity of the grating corresponds to 5-μm-wide storage regions separated by 5-μm-wide implanted regions. A simple electrical model for the correlator gate appears in Fig. 5, while Fig. 6 shows experimental C–V curves derived from an unimplanted wafer, a wafer implanted over its entire surface area, and a grating structure wafer. (The rise in the capacitance of the grating structure near -8.0 V is caused by lateral effects.) It is apparent from the curves in Fig. 6, that one can select a bias voltage between -1.0 and -10.0 V such that the inverted storage (nonimplanted) regions will be electrically isolated from one another by depletion regions in the implanted areas. This is the desired result as illustrated schematically in Fig. 7. The implant-isolated storage regions, however, in contrast to those formed by charge injection and trapping at the ZnO/SiO_2 interface [32], are established by a repeatable, well-controlled fabrication process and simple selection of the proper operating gate bias.

Verification of Storage-Region Isolation

Subsequent to ion implantation, implant activation during thermal oxidation, and deposition of the shorting pad metallization, special gate-pattern test structures were formed directly on the oxidized silicon surface. The test

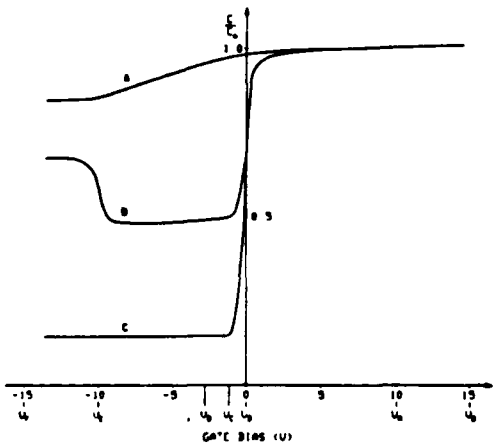

Fig. 6. Experimentally determined C-V characteristics derived from a (A) totally implanted (B) combined (grating) (C) non-implanted wafer. (V_A, V_B, etc. refer to the curves in Fig. 8).

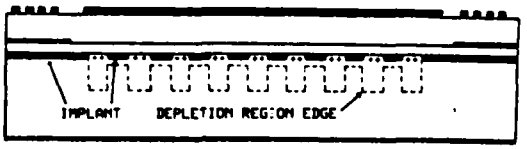

Fig. 7. Schematic of charge storage regions (induced junctions) established beneath the gate of the correlator. Plus signs denote inversion layer charge.

structures were subjected to a post-metallization anneal at 480°C for 5 min to minimize the SiO_2–Si interface state concentration. Capacitance-versus-time (C–t) transient measurements were then performed on the SiO_2–Si system in order to determine the storage capability of the grating, and to examine the effectiveness of the implant in isolating the storage regions.

The C–t transient results can be explained readily with the aid of Figs. 6 and 8. Fig. 8 shows a series of capacitance-versus-time characteristics of the grating region when pulsed from an equilibrium state at $V_G = V_o$ (accumulation) to various voltages (V_A, V_B, $\cdots$, V_F) labeled in Fig. 6. Trace A shows the result of pulsing the capacitor from the accumulation reference bias V_o, to an applied bias which is still in accumulation. As expected, there is no change in capacitance with time. Similarly for curve B, when both the storage and isolation regions are depleted, the $t > 0$ capacitance is time independent, but is lower because of the increased depletion widths of the two regions. Once the device is pulsed such that the nonimplanted region beneath the gate is inversion biased (curve C), the sudden pulse causes a deep depletion condition in the nonimplanted region with an accompanying finite relaxation time back to equilibrium. The difference in the C–t transient of curves C and D is that a larger negative pulse causes a greater degree of depletion in the implanted region and also a greater deep depletion width in the nonimplanted regions. After relaxation, the nonimplanted depletion widths remain at their maximum values. However, the total equilibrium capacitance is lower due to the larger

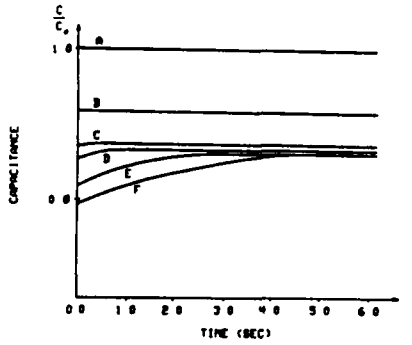

Fig. 8. Capacitance versus time (C–t transient) results for applied pulses described in Section II.

depletion width in the implanted region. Once the gate is pulsed from accumulation to a bias that tends to invert both the implanted and nonimplanted regions, the total capacitance always relaxes to the same minimum value as exemplified by curves E and F. This is true even though a larger negative pulse depletes the capacitors farther and for a longer time. The existence of a biasing range where the device relaxes to a decreasing final capacitance, followed by a biasing range where the final capacitance is always the same independent of bias, is direct verification of the underlying concept of the device: implant isolation of the storage regions. The biasing range over which the device relaxes to a decreasing final capacitance corresponds, of course, to the set of biases used in the normal operation of the storage correlator.

III. The Writing Process

Several methods for writing a reference signal into the storage regions of a device have been demonstrated including the flash mode [29] and various RF writing techniques [40]; we limit ourselves to the RF gate-acoustic writing mode for the implant-isolated storage correlator. The RF gate-acoustic writing method involves the application of an RF signal of short duration to the gate of the correlator while the reference signal to be stored is propagating beneath the gate. The resultant electrical potential in the gate region during the writing process has components of potential due to the acoustic reference signal, $V_a(t)\cos(\omega t - kz)$, (launched by a transducer) and the writing signal, $V_g(t)\cos\omega t$, applied to the gate. Both signals contribute to the total gate potential associated with the writing process, which is given by

$$V_S(z, t) = \sqrt{v_a^2 + 2v_a v_g \cos kz + v_g^2}\cos(\omega t - \phi) \quad (1)$$

where

$$\phi = \tan^{-1}\left(\frac{v_a \sin kz}{v_g + v_a \cos kz}\right). \quad (2)$$

Here v_a and v_g are the acoustic signal and gate signal potentials referenced to the gate [41]. As will be described below, $V_S(z, t)$ determines the surface charge density during a write sequence for any (z, t).

In this section a simple model is presented to describe the information storage process. To gain physical insight into the operation of a storage array, we first examine the response of the inversion layer charge and depletion capacitance of a single element of the storage region to a narrow (much shorter than one RF period) pulse applied to the gate. After analyzing the effect of a narrow pulse, each period of the RF signal of (1) is treated as a discretized sequence of narrow pulses. Using this discretized representation, the charge storage in response to any time varying writing signal can be estimated.

Charge Storage

Consider the effect upon a single storage region resulting from the application of a narrow positive pulse at the gate of a device that is biased for normal operation. Under equilibrium inversion conditions there is a maximum depletion width in the silicon. Applying a positive pulse of short duration to the gate while it is under equilibrium inversion bias will cause the storage-region depletion width to narrow by some amount, depending on the pulse amplitude and duration. At the same time, minority carrier holes in the inversion layer will be injected into the semiconductor depletion region, where some will recombine. Termination of this pulse causes the depletion width to instantaneously assume a new value equal to its equilibrium width plus an increment dependent upon the amount of minority carriers which recombined during the pulse. The change in depletion width changes the capacitance of the storage region, thereby contributing to signal storage in much the same way as in a p–n diode memory correlator.

In a quantitative description of the charge storage process, some assumptions have been made regarding the recombination and generation of minority carriers in the silicon. Here it is assumed that the recombination rate of injected holes, crucial to information storage, can be modeled by an effective recombination lifetime τ_R. Moreover, the generation of carriers during a narrow negative pulse (part of the negative going portion of the writing cycle) can be neglected because, as is obvious from the lengthy storage times, the return to equilibrium is very slow compared to the writing recombination rate. Surface states, traps in the semiconductor and ZnO, and charges in the oxides will also be neglected because they complicate the analysis without offering any insight into the writing process. With the stated assumptions, a quantitative description of the charge storage process has been performed for a single storage region.

As discussed in Section II, proper operation of this device is dependent upon the selection of an appropriate operating point gate bias. Assuming that a bias of V_G has been applied to the gate, one can, using the δ-depletion approximation [42], calculate the inversion layer charge at the silicon surface. Because the ZnO layer is only semi-insulating, the dc charge applied to the gate is readily injected into the ZnO film and is subsequently stored in traps adjacent to the ZnO-SiO_2 interface; i.e., under steady-state conditions a virtual gate is formed at the ZnO-SiO_2 interface [37]. The ZnO layer, therefore, can be neglected when calculating the equilibrium minority carrier inversion layer charge density, in which the magnitude is given by

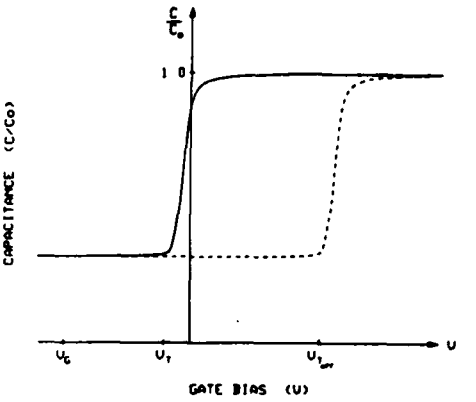

Fig. 9. C-V characteristics of a typical MIS capacitor (solid curve) and an MZOS capacitor exhibiting charge injection into the ZnO.

$$Q_{ss} = C_0\left[V_G - \frac{2kT}{q}U_F - \frac{qN_D}{C_0}\sqrt{\frac{4\kappa_s\epsilon_0}{qN_D}\frac{kT}{q}|U_F|}\right] \quad (3)$$

where C_0 is the capacitance (per unit area) of the SiO_2 layer, N_D is the background doping level of the n-type silicon substrate, and U_F is the substrate doping parameter. The dielectric constant of the silicon is represented by κ_s, the temperature by T, ϵ_0 is the permittivity of free space, and k is Boltzmann's constant. The constant U_F is given by

$$U_F = -\ln\left(\frac{N_D}{n_i}\right) \quad (4)$$

where n_i is the intrinsic carrier concentration.

Due to the localization of injected charge at the ZnO-SiO_2 interface, the equilibrium inversion layer charge under dc bias is independent of the ZnO layer capacitance. However, this is not true of the inversion-layer charge density when there are rapid changes in the gate bias. For RF signals in the frequency range of interest, voltage changes are too fast for the gate-injected electrons to follow the applied signal. Hence the capacitance of the ZnO layer must be included in any calculation of the redistributed surface charge. The condition just described can be visualized more easily with the aid of Fig. 9. In this figure, the solid curve represents a normal C–V characteristic for an n-type semiconductor, and V_G is the bias point. In a normal MOS capacitor one would have to pulse the gate to some bias greater than V_T to move out of inversion and into depletion. In the case of a correlator with an injecting ZnO film, however, the gate must be pulsed to $V_{T_{eff}}$ (on the dashed curve) to be at the edge of inversion. For comparison to the redistributed charge it is therefore more convenient to rewrite the equilibrium inversion layer charge density (3) for a given gate bias V_G in terms of $V_{T_{eff}}$ and

C_I (the series combination of the ZnO and SiO_2 capacitances). The resulting equivalent expression for Q_{seq} is given by

$$Q_{seq} = C_I\left[V_G + V_{T_{eff}} - \frac{2kT}{q}U_F - \frac{qN_D}{C_I}\sqrt{\frac{4\kappa_s\epsilon_0}{qN_D}\frac{kT}{q}|U_F|}\right] \quad (5)$$

where

$$C_I = \frac{C_{SiO_2}C_{ZnO}}{C_{SiO_2} + C_{ZnO}}. \quad (6)$$

The analysis of the charge storage process deals with the redistribution of this surface charge in response to an applied signal.

The application to the gate of a narrow positive pulse of amplitude V_A will cause a portion of the equilibrium surface charge to be injected into the semiconductor, where some of it will recombine. The amount of charge which recombines per pulse is dependent upon the pulse amplitude, pulse duration, the minority carrier recombination rate, and the inversion layer charge available prior to each pulse. Repeated applications of such a pulse within an interval that is short compared to the device storage time (-1 s) eventually leads to a steady-state deep depletion condition beneath the gate where the new inversion layer surface charge density Q_A saturates at

$$Q_A = C_I\left[V_G - V_A + V_{T_{eff}} - \frac{2kT}{q}U_F - \frac{qN_D}{C_I}\sqrt{\frac{4\kappa_s\epsilon_0}{qN_D}\frac{kT}{q}|U_F|}\right]. \quad (7)$$

For a given V_A, the maximum charge storage by one storage region in the implant-isolated correlator is therefore

$$\Delta Q = Q_{seq} - Q_A = C_I V_A. \quad (8)$$

Assuming an effective recombination lifetime, the application of a dc pulse of amplitude V_A and arbitrary duration t_p changes the inversion layer charge by an amount

$$\Delta Q_s = C_I V_A(1 - e^{-t_p/\tau_R}). \quad (9)$$

The expression for the inversion layer surface charge as a function of gate bias, applied pulse magnitude, and applied pulse duration is given by

$$Q_s(V_G, V_A, t_p) = Q_{seq} - C_I V_A(1 - e^{-t_p/\tau_R}). \quad (10)$$

If one were to pulse the device again immediately after the application of the first pulse, the starting inversion layer minority carrier density would be $Q_s(V_G, V_A, t_p)$ instead of Q_{seq}. The subsequent surface charge after additional pulses would be dependent upon the pulse durations as well as the pulse amplitudes.

As mentioned earlier, the change in surface charge caused by recombination during a positive pulse of duration t_p results in an increase in the depletion width of the storage regions; the new depletion width is given by

$$W(V_G, V_A, t_p) = \frac{\kappa_s\epsilon_0}{C_0}\left[-1 + \left(1 + \frac{V_G - \frac{Q_s(V_G, V_A, t_p)}{C_0}}{V_\Delta}\right)^{1/2}\right] \quad (11)$$

where

$$V_\Delta = \frac{\kappa_s\epsilon_0 qN_D}{2C_0^2}. \quad (12)$$

The modified depletion width corresponds to a decreased capacitance given by

$$C(V_G, V_A, t_p) = \frac{C_I}{1 + \frac{C_I}{C_0}\left[-1 + \left(1 + \frac{V_G - \frac{Q_s(V_G, V_A, t_p)}{C_0}}{V_\Delta}\right)^{1/2}\right]}. \quad (13)$$

Thus far we have described a method for determining the change in the depletion capacitance of a single-storage region in response to a narrow pulse applied to the device gate. To elaborate on the writing process, it is necessary to determine the effect of a time varying signal on the several hundred storage regions. That is, for a complete description of the writing function, one must define the depletion capacitance (stored charge) as a function of time and position. The treatment of a time varying signal is given in the Appendix for a signal represented by a sequence of pulses of finite duration.

Effective Recombination Lifetime

As described in the previous section, the amount of charge stored in the gate region of the device is dependent upon the amplitude and duration of the write signal, the effective recombination lifetime, and many parameters which are determined by the materials used. In this section an experimental method is presented for determining the effective recombination lifetime for the correlator.

To obtain the desired correlation output, one applies the RF signal to be correlated at the gate electrode (gate-to-acoustic reading mode). This process is analogous to the reading process in a p–n diode memory correlator [40]. Due to the spatially varying depletion capacitance, electric fields are established in the ZnO film which excite contrapropagating acoustic signals representing the convolution and correlation of the stored reference signal with the applied reading signal. Furthermore, it can be shown that the correlation output voltage is directly proportional to

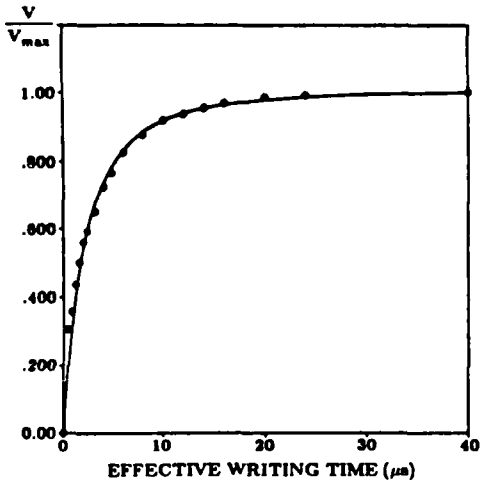

Fig. 10. Normalized correlation output voltage versus effective writing time. Solid curve corresponds to an effective minority carrier lifetime of $\tau_R = 0.67$ μs.

the amount of stored charge in the device. Therefore one can determine the effective recombination lifetime by fitting the predicted stored-charge dependence of (A3) to the actual correlation output versus writing time.

To observe the variation of correlation output with write time, an experiment was performed using the gate-acoustic writing mode and the gate-to-acoustic reading mode. The reference and reading signals were of 1.0-μs duration and the writing signal duration was 0.4 μs. To vary the writing time, multiple writing sequences were performed in rapid succession prior to each reading sequence. The number of successive writes determined the effective writing time (400-ns writing pulse times the number of writes prior to each read). The writes were performed 20 μs apart so any storage region relaxation between write pulses can be ignored. The experimental variation of correlation output versus write time is seen in Fig. 10. All values are normalized to the maximum value of correlation output. (It should be noted that in this experiment the time between readouts was several seconds to ensure sufficient decay of the stored signal before initiating a new write sequence.) The solid curve represents the predicted dependence of the correlation output voltage for an effective recombination lifetime of $\tau_R = 0.67$ μs as computed for the discretized sinusoidal approximation.

IV. Operational Characteristics

In this section we present experimental results for the correlation of two 1.0-μs RF bursts in order to examine correlator storage time, dynamic range and efficiency. All correlation measurements were performed using the RF gate-acoustic writing mode and the gate-to-acoustic reading mode. It should be pointed out that the implant-isolated storage correlator presented in this paper is bias-stable; that is, results of all correlation measurements are totally repeatable at any time without any special precautions, irrespective of the previous gate bias.

A key feature of the implant isolated correlator device is the time the device is capable of storing a reference

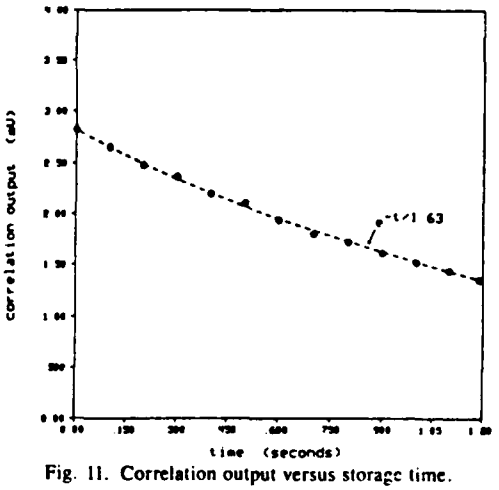

Fig. 11. Correlation output versus storage time.

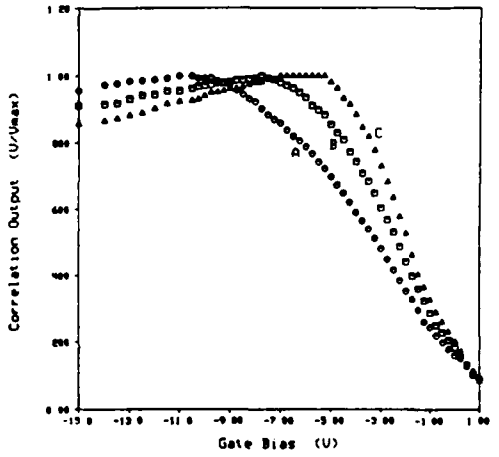

Fig. 12. Correlation output versus gate bias for different read-write power level combinations, where *A* denotes $P_W = 40.1$ dBm, and $P_R = 36.7$ dBm; *B* denotes $P_W = 37.1$ dBm and $P_R = 33.7$ dBm; and *C* denotes $P_W = 34.1$ dBm and $P_R = 30.7$ dBm.

signal. Fig. 11 displays the correlation output versus storage time; the data points fall along the dashed curve which corresponds to a 3-dB storage time of 0.56 s. Although this is certainly a long storage time compared to other previous MZOS correlator configurations, with advanced fabrication procedures it is not unreasonable to expect storage times of at least several seconds.

A plot of normalized correlation output versus gate bias is shown in Fig. 12 for three different values of read-write power level combinations. It is seen that for gate biases less than a certain value, the correlation output always remains within 85 percent of its maximum. This indicates a very wide bias range over which one may operate the device without significant degradation of the output signal. Based on theoretical considerations, one might expect that once the dc gate bias was sufficiently large to invert not only the storage regions, but also the ion implanted separation (and lateral) regions, then the lateral flow of inversion layer minority carriers from implanted regions surrounding the storage areas would eliminate the stored signal. The experimental results presented, however, indicate that the implanted region is of insufficient area to

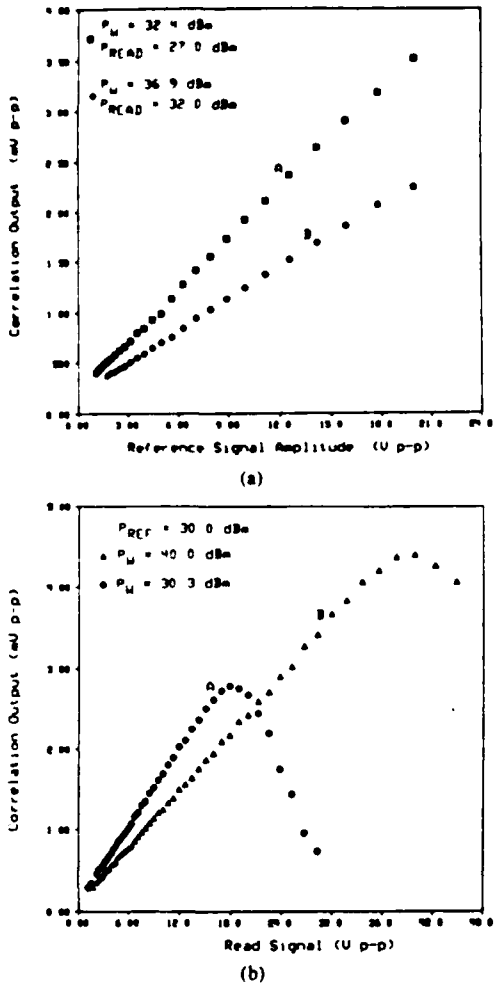

Fig. 13. (a) Correlation output versus reference signal amplitude. (b) Correlation output versus read signal amplitude.

supply the signal-eliminating flow of minority carriers. The top surface of the device after sawing and mounting extends approximately 1 mm to either side of the 1-mm-wide gate. This area is subject to lateral effects and should contribute to the overall relaxation, but it is apparently too small to degrade the output significantly.

An RF writing signal of 140 ns (18 cycles) was found to produce the highest correlation output, and this writing pulse duration was used when performing the correlation measurements shown in Fig. 13. Fig. 13(a) shows the correlation output versus the reference signal amplitude and the result is linear over a 25-dB range in correlator output power. The correlation output versus read pulse power can be seen in Fig. 13(b). Here again the dynamic range of the device is approximately 25 dB. In all measurements the correlation efficiency is between -100 and -110 dBm. The efficiency and dynamic range of this device are lower than expected. ZnO film quality during this particular sputter produced a delay line insertion loss some 14 dB more than in previous devices with the same dimensions. (The same was true for nonimplanted test structures.) A better piezoelectric film should upgrade both figures of merit into the range of previously reported monolithic memory correlators.

IV. Conclusion

A monolithic MZOS surface acoustic wave memory correlator that utilizes ion implantation to confine induced junction storage regions has been presented. The storage time capability of the device before fabrication is completed has been demonstrated by means of a pulsed capacitance-versus-time experiment. A simple model of the writing process was detailed which allows one to determine an effective minority carrier lifetime for the inversion layer charge. It has been demonstrated that 3 dB storage times in excess of 0.5 s are achievable with the promise of signal storage up to several seconds. Finally, this device exhibits bias stability, making the implant isolated storage correlator an attractive device for use as an on-chip circuit element.

Appendix

For a single pulse applied to a storage region one has, after a rectangular pulse of amplitude V_1 and duration Δt_1, a modified surface charge density of Q_1 given by

$$Q_1 = Q_{seq} - C_I V_1 (1 - e^{-\Delta t_1/\tau_R}). \tag{A1}$$

If one applies another pulse of amplitude V_2 and duration Δt_2 at some instant immediately after turning off pulse V_1, then the surface charge density is given by

$$\begin{aligned} Q_2 &= Q_{seq} - C_I V_2 \\ &\quad + [Q_1 - (Q_{seq} - C_I V_2)]\, e^{-\Delta t_2/\tau_R} \\ &= Q_{seq} - C_I V_2 (1 - e^{-\Delta t_2/\tau_R}) \\ &\quad - C_I V_1\, e^{-\Delta t_2/\tau_R} (1 - e^{-\Delta t_1/\tau_R}). \end{aligned} \tag{A2}$$

Similarly, with the application of numerous narrow pulses of amplitudes V_i, one can replicate any time varying signal. If one discretizes the desired signal into uniform increments of duration Δt, one can determine the surface charge density for the application of a signal $N\Delta t$ long by

$$Q_N = Q_{seq} - C_I (1 - e^{-\Delta t/\tau_R}) \left(\sum_{i=1}^{N} V_i\, e^{-(n-i)\Delta t/\tau_R} \right), \qquad V_i > 0. \tag{A3}$$

Furthermore, in addition to the constraint that V_i must be positive, as the storage depletion width expands, only pulses sufficiently large to contribute to further charge storage are used in the computation of Q_N.

Acknowledgment

The authors wish to thank M. Young and T. Miller for the ion implantation of the devices as well as G. MaGee, S. Phillips, and T. Corbin of the Naval Avionics Center in Indianapolis, IN, for their assistance in making photomasks.

REFERENCES

[1] M. R. Melloch and R. S. Wagers, "Wide-band monolithic GaAs convolver and memory correlator," *Appl. Phys. Lett.*, vol. 43, no. 1, pp. 48-50, July 1, 1984.

[2] ——, "Controlled diode profiling for GaAs strip-coupled correlators," *IEEE Elec. Dev. Lett.*, vol. EDL-5, no. 5, pp. 136-138, May 1984.

[3] F. S. Hickernell, "DC triode sputtered zinc oxide surface elastic wave transducers," *J. Appl. Phys.*, vol. 44, no. 3, pp. 1061-1071, Mar. 1973.

[4] R. L. Gunshor, S. J. Martin, and R. F. Pierret, "Surface acoustic wave devices on silicon," in *Proc. 1982 Int. Conf. Solid State Devices*, 1982. Also see *Jap. J. Appl. Phys.*, vol. 22, no. 1, pp. 37-41, 1983.

[5] G. S. Kino, "Zinc oxide on silicon acoustoelectric devices," in *Proc. 1979 IEEE Ultrason. Symp. Proc.*, 1979, pp. 900-910.

[6] K. M. Lakin, J. Liu, and K. Wang, "Aluminum nitride on sapphire," in *Proc. 1983 IEEE Ultrason. Symp. Proc.*, 1974, pp. 302-306.

[7] L. G. Pearce, R. L. Gunshor, and R. F. Pierret, "Aluminum nitride on silicon surface acoustic wave devices," *Appl. Phys. Lett.*, vol. 39, no. 11, pp. 878-879, 1981.

[8] K. Tsubouchi and N. Mikoshiba, "Zero temperature coefficient SAW delay line on AIN epitaxial films," in *Proc. 1983 IEEE Ultrason. Symp.*, 1983, pp. 299-310.

[9] C. W. Lee and R. L. Gunshor, "Nonlinear interaction of acoustic surface waves from coupling to charge carriers," *J. Appl. Phys.*, vol. 44, no. 11, pp. 4807-4812, Nov. 1973.

[10] W. C. Wang, "Convolution of surface waves in a structure of semiconductor on $LiNbO_3$," *Appl. Phys. Lett.*, vol. 20, no. 10, pp. 389-392, May 15, 1972.

[11] P. Das, M. N. Araghi, and W. C. Wang, "Convolution of signals using surface wave delay line," *Appl. Phys. Lett.*, vol. 21, no. 4, pp. 152-154, Aug. 1972.

[12] M. Yamanishi, T. Kawamura, and Y. Nakayama, "Acoustic Surface Wave Convolver Using Nonlinear Interaction in a Coupled PZT-Si System," *Apply Phys. Lett.*, vol. 21, no. 4, pp. 146-148, Aug. 1972.

[13] G. S. Kino, W. R. Shreve, and H. R. Gautier, "Parametric interactions, of rayleigh waves," in *Proc. 1972 IEEE Ultrason. Symp.*, 1972, pp. 285-287.

[14] R. L. Gunshor, "The interaction between semiconductors and acoustic surface waves—A review," *Solid-State Electron.*, vol. 18, pp. 1089-1093, 1975.

[15] R. W. Ralston, J. H. Cafarella, S. A. Reible, and E. Stern, "Improved acoustoelectric schottky-diode/$LiNbO_3$ memory correlator," in *Proc. 1977 IEEE Ultrason. Symp.*, 1977, pp. 472-477.

[16] T. Shiosaki, T. Yamamoto, and A. Kawabata, "Higher order mode rayleigh waves propagating on ZnO/substrate structures," in *Proc. 1977 IEEE Ultrason. Symp.*, 1977, pp. 814-818.

[17] J. K. Elliott, R. L. Gunshor, R. F. Pierret, and A. R. Day, "A wide-band SAW convolver utilizing Sezawa waves in the Metal-ZnO-SiO_2-Si configuration," *Appl. Phys. Lett.*, vol. 32, no. 9, pp. 515-516, May 1978.

[18] F. C. Lo, R. L. Gunshor, and R. F. Pierret, "Monolithic (ZnO) Sezawa-mode p-n diode-array memory correlator," *Appl. Phys. Lett.*, vol. 34, no. 11, pp. 725-726, June 1979.

[19] S. Minigawa, T. Okamoto, R. Asai, and Y. Sato, "Efficient monolithic ZnO/Si Sezawa wave convolver," in *Proc. 1982 IEEE Ultrason. Symp.*, 1982.

[20] J. E. Bowers, B. T. Khuri-Yakub, and G. S. Kino, "Monolithic Sezawa wave storage correlators and convolvers," in *Proc. 1980 IEEE Ultrasonics Symposium Proceedings*, 1980, pp. 98-103.

[21] R. L. Gunshor and C. W. Lee, "Generation of a surface acoustic wave correlation echo from coupling-to-charge carriers," *Appl. Phys. Lett.*, vol. 21, no. 1, pp. 11-12, July 1972.

[22] M. Luukkala and G. S. Kino, "Convolution and time inversion using parametric interactions of acoustic surface waves," *Appl. Phys. Lett.*, vol. 18, no. 9, pp. 393-394, May 1971.

[23] A. Bers and J. H. Cafarella, "Surface state memory in surface acoustoelectric correlator," *Appl. Phys. Lett.*, vol. 25, no. 3, pp. 133-135, August 1974.

[24] H. Hayakawa and G. S. Kino, "Storage of acoustic signals in surface states in silicon," *Appl. Phys. Lett.*, vol. 25, pp. 178-180, 1974.

[25] C. Maerfeld, Ph. Defranould, and P. Tournois, "Acoustic storage and processing device using p-n diodes," *Appl. Phys. Lett.*, vol. 27, no. 11, pp. 577-578, Dec. 1975.

[26] H. C. Tuan, B. T. Khuri-Yakub, and G. S. Kino, "A new zinc-oxide-on-Silicon Monolithic Storage Correlator," in *Proc. 1977 IEEE Ultrason. Symp.*, pp. 496-499, 1977.

[27] P. G. Borden, R. Joly, and G. S. Kino, "Correlation With the Storage Convolver," *IEEE Ultrason. Symp. Proc.*, pp. 348-351, 1976.

[28] F. C. Lo, R. L. Gunshor, R. F. Pierret, and J. K. Elliott, "Separation of storage effects in monolithic p-n diode correlators," *Appl. Phys. Lett.*, vol. 33, no. 11, pp. 903-905, Dec. 1, 1978.

[29] K. A. Ingebrigtsen, R. A. Cohen, and R. W. Mountain, "A Schottky-diode acoustic memory and correlator," *Appl. Phys. Lett.*, vol. 26, no. 11, pp. 596-598, June 1975.

[30] K. A. Ingebrigtsen, "The Schottky diode acoustoelectric memory and correlator: A novel programmable signal processor," *Proc. IEEE*, vol. 64, no. 5, pp. 764-769, May 1976.

[31] W. C. Wang, "Physical processes of SAW Schottky-diode memory correlator," *Electron. Lett.*, vol. 12, pp. 105-106, 1976.

[32] K. C. K. Weng, R. L. Gunshor, and R. F. Pierret, "Induced junction monolithic zinc oxide-on-silicon storage correlator," *Appl. Phys. Lett.*, vol. 40, pp. 71-73, 1982.

[33] J. K. Elliott, R. L. Gunshor, R. F. Pierret, and K. L. Davis, "Characteristics of zinc-oxide-silicon surface wave convolvers for optical imaging and memory," in *Proc. IEEE Ultrason. Symp.*, 1975, pp. 141-143.

[34] K. L. Davis, "Properties of the MZOS surface wave convolver configuration," *IEEE Trans. Electron Devices*, vol. 23, no. 6, pp. 554-559, June 1976.

[35] L. A. Coldren, "Effect of bias field in a zinc-oxide-on-silicon acoustic convolver," *Appl. Phys. Lett.*, vol. 25, no. 9, pp. 473-475, Nov. 1974.

[36] J. K. Elliott, R. L. Gunshor, R. F. Pierret, and K. L. Davis, "Zinc-oxide-silicon monolithic acoustic surface wave optical image scanner," *Appl. Phys. Lett.*, vol. 27, no. 4, pp. 179-182, Aug. 15, 1975.

[37] R. F. Pierret, R. L. Gunshor, and M. E. Cornell, "Charge injection in metal-ZnO-SiO_2-Si structures," *J. Appl. Phys.*, vol. 50, no. 12, pp. 8112-8124, Dec. 1979.

[38] M. R. Melloch, R. L. Gunshor, and R. F. Pierret, "Single phase and balanced separate comb transducer configurations in a ZnO/Si SAW structure," *IEEE Trans. Sonics Ultrason.*, vol. 28, no. 1, pp. 55-58, 1982.

[39] I. Yao, "High-performance elastic convolver with parabolic horns," in *Proc. 1980 IEEE Ultrason. Symp.*, 1980.

[40] Ph. Defranould, H. Gautier, C. Maerfeld, and P. Tournois, "p-n diode memory correlator," in *Proc. 1976 IEEE Ultrason. Symp.*, pp. 336-347, 1976.

[41] H. C. Tuan, J. E. Bowers, and G. S. Kino, "Theoretical and experimental results for monolithic SAW memory correlators," *IEEE Trans. Sonics Ultrason.*, vol. 27, no. 6, pp. 360-369, Nov. 1980.

[42] R. F. Pierret, *Modular Series on Solid State Devices*, (*Field Effect Devices*, vol. 4). New York: Addison-Wesley, 1983, pp. 32-36.

Stephen Schwartz was born in Boston, Massachusetts on October 24, 1959. He received the B.S., M.S., and Ph.D. degrees in electrical engineering from Purdue University, West Lafayette, IN, in 1981, 1982, and 1985, respectively.

He is currently involved in postdoctoral research at Purdue University. His research interests include zinc oxide-on-silicon surface acoustic wave resonators, correlators, and filters.

Dr. Schwartz is a member of Tau Beta Pi, Eta Kappa Nu, and Sigma Xi.

Robert L. Gunshor was born in New York in 1935. He received the B.E.E. degree from New York University, the M.S.E degree from Union College, Schenectady, NY, and the Ph.D degree from Rensselaer Polytechnic Institute, Rensselaer, NY, all in electrical engineering.

He is Professor of Electrical Engineering at Purdue University. He has worked on microwave tubes, plasma waves, and Gunn devices. His current interests include layered thin-film SAW devices and the growth and evaluation of the II-VI semiconductor quantum well structures by molecular beam epitaxy.

Dr. Gunshor is a member of the American Physical Society, Sigma Xi, and is an associate editor of the IEEE TRANSACTIONS ON SONICS AND ULTRASONICS.

Robert F. Pierret (M'72-SM'84), photograph and biography not available at the time of publication.

APPENDIX B

SAW RESONATORS INSENSITIVE TO IDT POSITION

S. S. Schwartz, S.J.Martin*, R. L. Gunshor, S. Datta, and R. F. Pierret

School of Electrical Engineering, Purdue University
West Lafayette, Indiana 47907

Abstract

A theoretical analysis of the ZnO-on-Si surface acoustic wave mode conversion resonator indicates that optimum performance can be attained irrespective of transducer location between reflector arrays. That is, a single transducer of Rayleigh or Sezawa periodicity can be placed anywhere between properly spaced mode conversion gratings and it will couple optimally to a standing wave of the same periodicity. An extension of the theory allows one to fabricate both one-port and two-port resonators with non-critical spacing between the transducers and the gratings. Experimental verification of the position independent behavior is presented for one-port and two-port devices.

I. Introduction

Since the introduction of the first surface acoustic wave (SAW) resonator by Ash[1], this class of devices has been useful in performing many signal processing tasks. Among other applications, these rugged, high Q elements have been used as accelerometers[2], pressure sensors[3], vapor sensors[4], narrowband filters[5,6,7,8], and frequency control elements for oscillators[9,10]. Although most SAW resonators constructed to date have been fabricated on single crystal substrates such as quartz and lithium niobate, a great deal of progress has been achieved in implementing SAW resonators in the $ZnO/SiO_2/Si$ layered medium configuration[11]. Like the single crystal resonators, these devices have demonstrated low insertion loss, high Q values[12], favorable aging characteristics[13], and temperature stability comparable to ST-quartz[14]. To exemplify some of these properties, the two-port transmission response of a SAW resonator in the $ZnO/SiO_2/Si$ configuration is shown in Fig. 1. The device, whose response is shown, was constructed in the temperature stable configuration with apodized transducers to eliminate undesirable transverse modes. The insertion loss of 4 dB is an indication of the high performance capability of SAW resonators in the layered configuration.

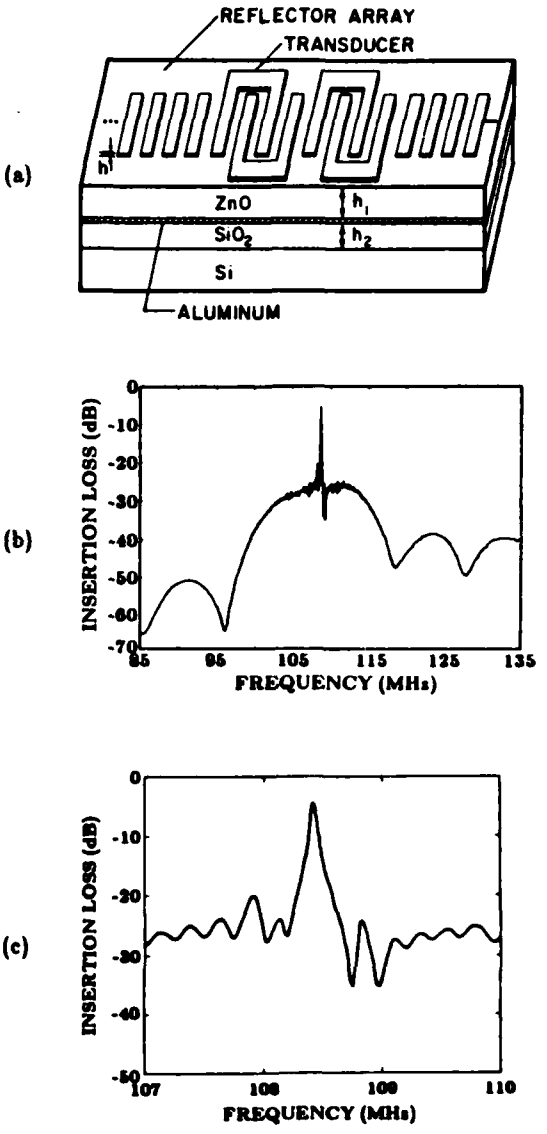

Fig. 1. (a) Schematic of a typical two-port $ZnO/SiO_2/Si$ SAW resonator. (b) Two-port transmission response for a ZnO-on-Si SAW resonator. (c) Two-port transmission response without transverse modes.

* Present address: Sandia National Laboratories, Albuquerque, New Mexico

0090-5607/84/0000-0229 $1.00 © 1984 IEEE

Recently, a new concept in ZnO-on-Si SAW resonators was reported[15] involving mode conversion between Rayleigh and Sezawa waves rather than single mode Bragg reflection for confinement of SAW energy. The first of these mode conversion devices were fabricated with the promise of high out-of-band rejection due to the relatively low cross coupling level between interdigital transducers (IDT's) of different periodicity. In this paper we present yet another advantage of this type of SAW resonator -- that of a relaxed spacing requirement between the transducers and the gratings. We demonstrate that the location of the standing waves in the device are determined by the position of the transducers and that regardless of transducer location, one will couple optimally to the resonant cavity.

Although a detailed description of the theory of operation of the mode conversion resonator will be published at a later time, we use this paper to present experimental verification of our predictions. Section II provides a description of the basic device structure and operation, followed by a brief outline of the device theory in Section III. We present experimental results in Section IV for resonators fabricated in both one-port and two-port configurations.

II. Device Structure

The mode conversion resonator developed by Martin et. al[15]. consists of the same basic features as a conventional single mode resonator (i.e. transducers and reflector arrays); it is dimensionally, however, very different. A schematic of a two-port version of the mode conversion resonator is shown in Fig. 2. The device consists of two interface transducers[16] between ion beam etched reflector arrays onto which a ZnO film, of sufficient thickness to support the Sezawa mode, has been deposited by rf diode sputtering. One transducer is of Rayleigh wave type with periodicity λ_R, and the other has Sezawa wave periodicity λ_S. The

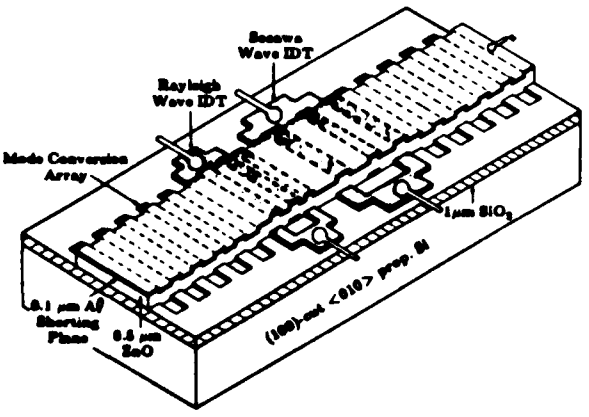

Fig. 2. Schematic of a two-port mode conversion resonator using both Rayleigh and Sezawa transducers.

periodicity of the reflector array, d, is determined by the mode conversion condition[17,18]

$$k_S + k_R = \frac{2\pi}{d} \quad , \tag{1}$$

where k_R and k_S are the Rayleigh and Sezawa wavenumbers respectively.

As previously described[15], the reflector array periodicity is chosen to satisfy Eq. 1 such that a wave of Rayleigh or Sezawa type incident upon a reflector will be back-scattered as a wave of the other type at the same frequency. That is, a wave launched by the Rayleigh transducer which impinges on a grating will be reflected as a Sezawa wave and, after traversing the cavity as a Sezawa wave, will be re-reflected by the opposite grating as a Rayleigh wave. (The same holds true for Sezawa waves converted to Rayleigh waves.) Because bi-directional transducers are used, the process occurs in both directions; when the total round trip phase shift of the multiply reflected waves is a multiple of 2π, standing Rayleigh and Sezawa wave patterns result and resonance is achieved. It is this 2π phase shift requirement which imposes a restriction on the separation between reflector arrays. More precisely, for resonance to occur, the separation, L_o, between inner edges of the mode converting arrays must be

$$L_o = md \quad , \tag{2}$$

where m is any integer and d is the array periodicity. When this condition has been satisfied one will couple optimally to the resonant cavity when each of the transducers is positioned such that its fingers are at locations of standing wave maxima of a wave with the same periodicity.

We will show that for mode conversion resonators, it is the placement of the transducers (between properly spaced gratings) which dictates the location of the standing wave pattern, irrespective of where the transducer is located between mode converting arrays. Furthermore, a transducer of Rayleigh or Sezawa type, placed randomly in the cavity will always couple optimally to the resonant modes. This is in marked contrast to a conventional SAW resonator where the grating periodicity and separation between gratings determine the location of the standing wave pattern and hence the placement of the transducers for optimal performance.

III. Operation

To examine the position independence of the mode conversion device we consider the resonant cavity in the absence of transducers. The two modes, A and B, depicted in Fig. 3 represent independent normal modes of the resonator. When the spacing between reflectors is such that the total round-trip phase shift for each mode (as a Rayleigh wave in one direction and a Sezawa wave in the other direction) is a multiple of 2π,

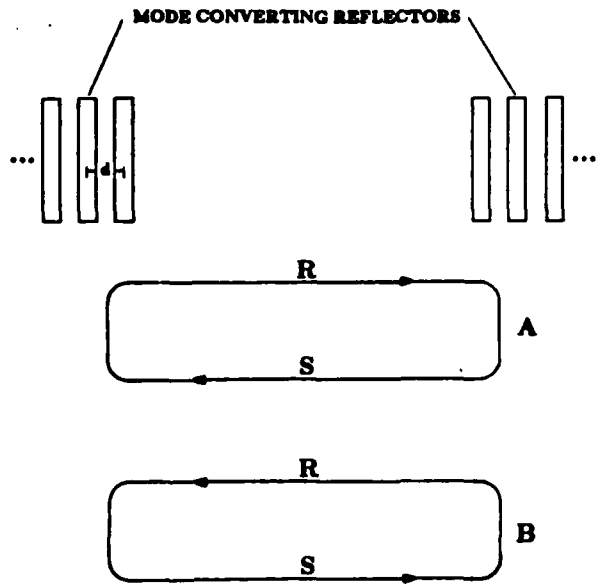

Fig. 3. Schematic of the mode conversion resonator cavity illustrating two independent resonant modes.

each of these independent modes is a resonant mode of the cavity. Unlike a conventional resonator whose resonant mode is a standing wave pattern, each of these resonant modes consists of travelling Rayleigh and Sezawa waves. The introduction of a transducer of either Rayleigh or Sezawa type serves to couple these modes together by fixing a finite phase relationship between them. It is this coupling of the resonant modes which ensures that the fingers of the transducer will be located at the positions of standing wave maxima of the wave with the same periodicity as the IDT. Any shift in the position of the IDT will cause the standing wave of the same periodicity to move along with the transducer irrespective of where it is positioned between reflectors. It is important to note that a standing wave of the other type will exist simultaneously, but a shift in position of the IDT will cause a disproportionate shift in the location of the other standing wave. In a one-port resonator the location of the other standing wave need not be considered since the transducer couples automatically to only one standing wave type. However, when coupling to both standing wave types in a two-port configuration, one must know the relative positions of both standing waves.

To couple optimally to this resonator through transducers of differing periodicity one can place a transducer of Rayleigh or Sezawa type anywhere between reflectors but must place the transducer of the other periodicity at one of a limited number of allowed positions which are determined by the location of the first IDT with respect to the reflector arrays. That is, in a two-port mode conversion resonator with transducers of different periodicity, the placement of one of the two IDT's is critical.

To fabricate a two-port resonator and still be able to exploit the positional independence of this structure, one must use transducers of the same periodicity which are spaced an integer number of half wavelengths from each other. As described above, placement of the first IDT guarantees the standing wave pattern location; this ensures maximum coupling to the same standing wave at the other transducer. As long as both transducers are spaced properly with respect to each other, the two-port device using identical IDT's will be position independent. Additionally, either a Rayleigh IDT pair or a Sezawa IDT pair may be used for this resonator.

IV. Experimental Results

To demonstrate the positional independence of the resonator response on IDT position, we fabricated both one-port and two-port mode conversion devices with different spacings between transducers and reflector arrays. Both types of devices were fabricated on (100) cut (<100> propagating) silicon substrates. The only changes between devices were the positions of the transducers between reflector arrays. All transducers used were of Sezawa type and had a periodicity of 35.5μm. The transducers for the one-port devices had nine finger-pairs while the transducers used in the two-port devices had five finger-pairs each. For both structures, the reflector arrays consisted of 400 ion beam etched grooves 1300 Å deep with a periodicity of 12.7 μm and a beamwidth of 1.5 mm. For the devices used in this experiment, the transducers and reflector arrays were defined on the top surface of the ZnO rather than at the ZnO/SiO_2 interface (Fig. 2) because equivalent coupling to both wave types was no longer necessary[15]. The array separation used in all devices was 0.762 mm which corresponds to 60 grating periods.

In the one-port mode conversion resonator we fabricated a series of devices with the transducer position varied by fractions of a Sezawa wavelength from the center of the cavity. The devices fabricated had transducers placed $\frac{n\lambda_S}{16}$ from the center of the reflectors with n = 0,1,2,...,7. Results of this experiment can be seen in Fig. 4 which shows the measured radiation conductance, G_a, for a number of transducer positions for the mode conversion resonator together with computed G_a values for conventional one-port resonators with the same spacings.

As is expected, in a conventional one-port structure with the same spacing, the resonant coupling condition greatly depends on the transducer placement between reflectors. In the mode conversion resonator structure, however, resonance as demonstrated by the enhanced radiation conductance, can be observed for any location of the IDT.

A similar experiment was performed for two-port mode conversion resonators with a fixed spacing of $10\lambda_S$ between centers of identical Sezawa transducers.

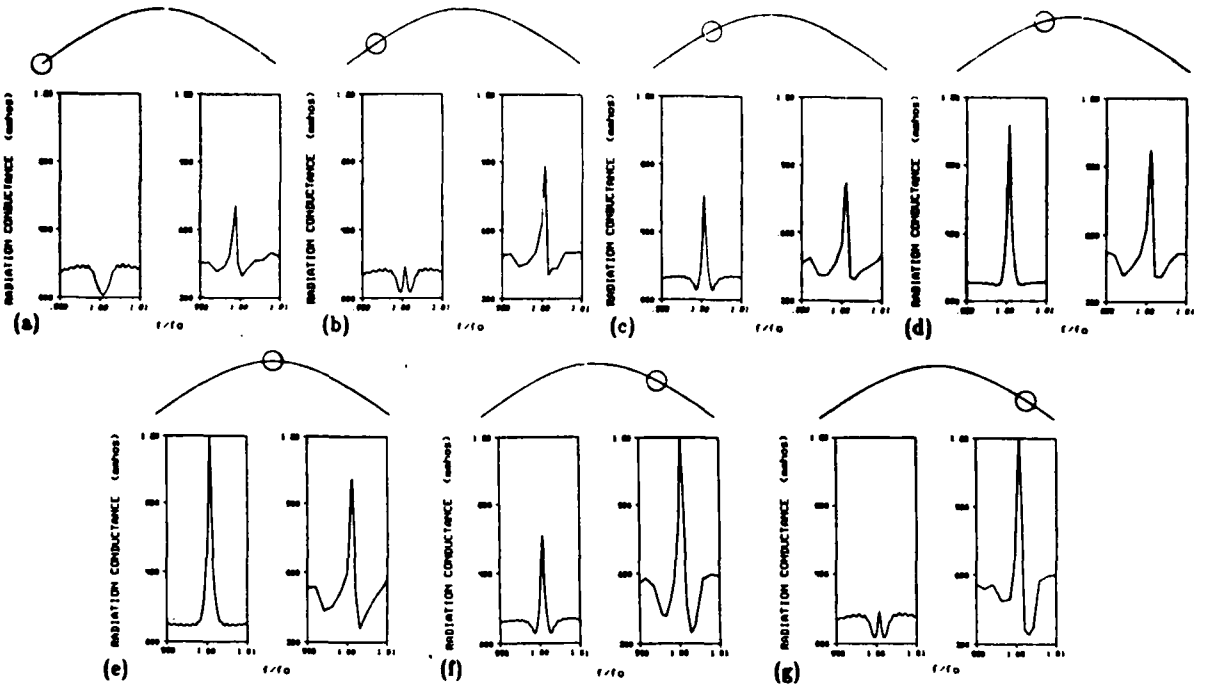

Fig. 4. Radiation conductance vs. frequency determined experimentally for one-port mode conversion resonators (right) and computed for conventional one-port resonators (left). In both results the transducer was displaced from the cavity center an amount $\frac{n\lambda_o}{16}$ for (a) n=0 (b) n=1 (c) n=2 (d) n=3 (e) n=4 (f) n=6 (g) n=7.

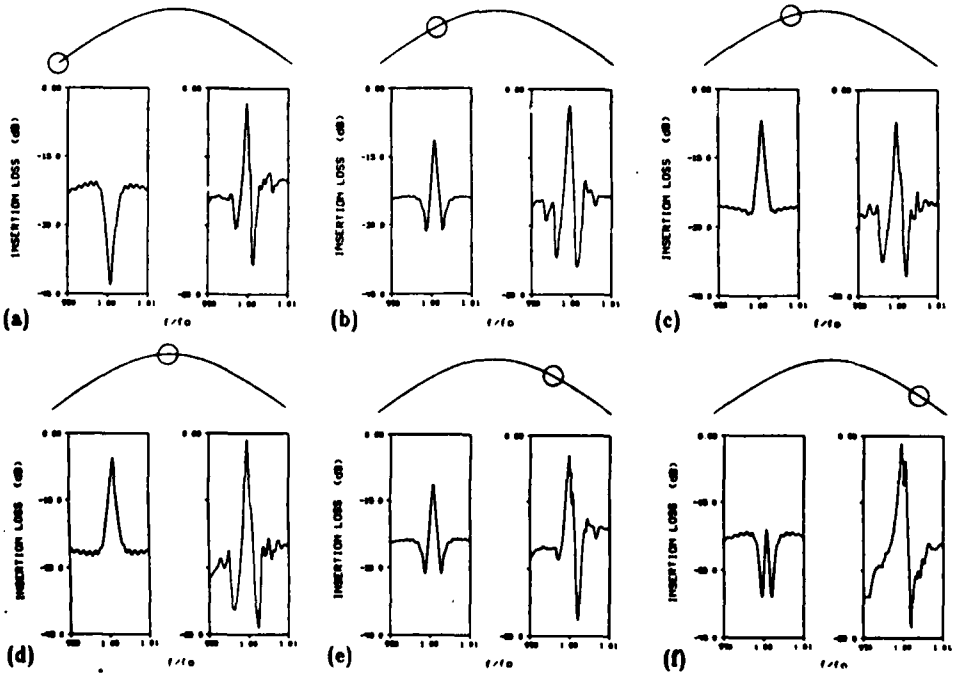

Fig. 5. Two-port transmission response vs. frequency determined experimentally for mode conversion resonators (right) and computed for conventional two-port resonators (left). In both devices, the transducer pair was displaced from the cavity center by an amount $\frac{n\lambda_o}{16}$ for (a) n=1 (b) n=2 (c) n=3 (d) n=5 (e) n=6 (f) n=7.

The midpoint of the pair of transducers was varied from the cavity center by the same fraction as in the one-port experiment; the results are shown in Fig. 5. Here again, the calculated response for a conventional device with the same dimensions was computed and plotted alongside the experimental results. It is evident that as the location of the transducer pair is moved within the cavity, there are drastic changes in the response of a conventional device (i.e. resonance and antiresonance) but the results for a two-port mode conversion resonator are almost invariant.

For both one-port and two-port device structures the resonant Q values were in the range 900-1500 but it should be noted that no attempt was made to optimize these resonators but rather to demonstrate the positional independence of the transducer placement. It should also be pointed out that in both one-port and two-port devices, slight variations in the device responses for different spacings are due to the fact that the standing Rayleigh wave pattern is not invisible to the Sezawa IDT's and some coupling will exist which will be different for each spacing chosen. This variation can be minimized by increasing the number of fingers per transducer.

V. Conclusions

We have defined a technique whereby one can fabricate SAW resonators whose response is independent of IDT positioning. Results have been presented for devices fabricated in both one-port and two-port configurations and comparisons have been made with conventional SAW resonators. Furthermore, the relaxed spacing requirement we have demonstrated allows one to more easily incorporate these devices into a standard monolithic IC fabrication process. The eased fabrication stems from the fact that a grating can be defined in the SiO_2 during an already existing etching step and the transducers can be defined during the final metallization step in a completely different plane with no need for a critical alignment.

Acknowledgements

The authors wish to thank S. Phillips, T. Corbin, and G. MaGee of the Naval Avionics Facility at Indianapolis for the photoplates used in these experiments as well as T. Miller and M. Young for their assistance in the fabrication of the devices.

This work was sponsored by the Air Force Office of Scientific Research under Grant No. AFOSR-83-0237.

References

1. E. A. Ash, *Surface Wave Grating Reflectors and Resonators, IEEE Symposium Microwave Theory and Techniques, Newport Beach, Calif.*, May 11-14, 1970.

2. S. J. Martin, R. L. Gunshor, R. F. Pierret, and G. Gorodetsky, "Uniaxially Strained $ZnO/SiO_2/Si$ SAW Resonators," *Electronics Letters*, vol. 18, no. 24, pp. 1030-1031, 25 November 1982.

3. P. Das, C. Lanzl, and H. F. Tiersten, "A Pressure Sensing Acoustic Surface Wave Resonator," *IEEE Ultrasonics Symposium Proceedings*, pp. 306-308, 1976.

4. S. J. Martin, K. S. Schweizer, S. S. Schwartz, and R. L. Gunshor, "Vapor Sensing by Means of a ZnO-on-Si Surface Acoustic Wave Resonator," *IEEE Ultrasonics Symposium Proceedings*, To be published in this issue.

5. R. Stevens, P. D. White, and R. F. Mitchell, "Stopband Level of 2-Port SAW Resonator Filters," *IEEE Ultrasonics Symposium Proceedings*, pp. 905-908, 1977.

6. R. V. Schmidt and P. S. Cross, "Externally Coupled Resonator-Filter (ECRF)," *IEEE Trans. on Sonics and Ultrasonics*, vol. SU-26, no. 2, pp. 88-92, March 1979.

7. R. L. Rosenberg and L. A. Coldren, "Scattering Analysis and Design of SAW Resonator Filters," *IEEE Trans. on Sonics and Ultrasonics*, vol. SU-26, no. 3, pp. 205-229, May 1979.

8. G. L. Matthaei, E. B. Savage, and F. Barman, "Synthesis of Acoustic-Surface-Wave-Resonator Filters Using Any of Various Coupling Mechanisms," *IEEE Trans. on Sonics and Ultrasonics*, vol. SU-25, no. 2, pp. 72-84, March 1978.

9. T. O'Shea, V. Sullivan, and R. Kindell, *Precision L-band SAW Oscillator for Satellite Application.*

10. R. D. Colvin, "UHF Acoustic Oscillators," *Microwave Journal*, pp. 22-33, November, 1980.

11. S. J. Martin, S. S. Schwartz, R. L. Gunshor, and R. F. Pierret, "Surface Acoustic Wave Resonators on a ZnO-on-Si Layered Medium," *J. Appl. Phys.*, vol. 54, no. 2, pp. 561-569, February 1983.

12. S. S. Schwartz, S. J. Martin, R. L. Gunshor, S. Datta, and R. F. Pierret, "SAW Resonators on Silicon with ZnO Limited to IDT Regions," *IEEE Ultrasonics Symposium Proceedings*, pp. 161-163, 1983.

13. S. J. Martin, R. L. Gunshor, M. R. Melloch, S. Datta, and R. F. Pierret, "Surface Acoustic Wave Mode Conversion Resonator," *IEEE Ultrasonics Symposium Proceedings*, 1982.

14. S. J. Martin, R. L. Gunshor, and R. F. Pierret, "High Q, Temperature Stable ZnO-on-Silicon SAW Resonators," *IEEE Ultrasonics Symposium Proceedings*, 1981.

15. S. J. Martin, R. L. Gunshor, M. R. Melloch, S. Datta, and R. F. Pierret, "Surface Acoustic Wave Mode Conversion Resonator," *Appl. Phys. Lett.*, vol. 43, no. 3, pp. 238-240, August 1983.

16. M. R. Melloch, R. L. Gunshor, C. L. Liu, and R. F. Pierret, "Interface Transduction in the ZnO–SiO_2–Si Surface Acoustic Wave Device Configuration," *Appl. Phys. Lett.*, vol. 37, no. 2, pp. 147-150, 15 July 1980.

17. M. R. Melloch, R. L. Gunshor, and R. F. Pierret, "Conversion of the Sezawa to Rayleigh Waves in the ZnO–SiO_2–Si Configuration," *IEEE Ultrasonics Symposium Proceedings*, 1981.

18. M. R. Melloch, R. L. Gunshor, and R. F. Pierret, "Sezawa to Rayleigh Mode Conversion in the ZnO-on-Si Surface Acoustic Wave device Configuration," *Appl. Phys. Lett.*, vol. 39, no. 6, pp. 476-477, September 1981.

APPENDIX C

Wide gap II-VI superlattices of ZnSe-$Zn_{1-x}Mn_xSe$

L. A. Kolodziejski, R. L. Gunshor, T. C. Bonsett, R. Venkatasubramanian, and S. Datta
School of Electrical Engineering, Purdue University, West Lafayette, Indiana 47907

R. B. Bylsma and W. M. Becker
Physics Department, Purdue University, West Lafayette, Indiana 47907

N. Otsuka
School of Materials Engineering, Purdue University, West Lafayette, Indiana 47907

(Received 21 March 1985; accepted for publication 29 April 1985)

In this letter we report the first growth of wide gap II-VI semiconductor superlattices of $Zn_{1-x}Mn_xSe$ ($0 < x < 0.51$). The superlattices are grown by molecular beam epitaxy. Bulk crystals of $Zn_{1-x}Mn_xSe$ ($0 < x < 0.57$) grown in the past have shown a predominance of the zincblende phase only up to $x = 0.3$; above this mole fraction a predominance of the hexagonal phase is observed. For the superlattices and epilayers reported here, only the zincblende phase (100) is present over the entire composition range investigated. Transmission electron microscopy shows clear evidence of the superlattice structure. Photoluminescence measurements of ZnSe epilayers show a dominant free-exciton feature while the $Zn_{1-x}Mn_xSe$ epilayers exhibit two distinct photoluminescence peaks. The relative intensities of band-to-band transitions and Mn-related transitions are somewhat comparable for the epilayers. However, the superlattices having ZnSe in the wells show virtually no Mn-related emission regardless of the mole fraction of Mn in the barrier layers indicating significant carrier confinement. The intensity of the band-to-band emission is two orders of magnitude more intense for the superlattices than the ZnSe epilayer at 6.5 K. The superlattices show a red shift of the photoluminescence peak which can be explained in terms of shifts in the band gaps due to the presence of strains.

Recently the growth of epilayers and superlattices of II-VI compounds and their alloys by molecular beam epitaxy (MBE) has attracted much attention. Two alloy systems have been reported so far, the narrow band-gap $Hg_{1-x}Cd_xTe$ system and the $Cd_{1-x}Mn_xTe$ system which has a band gap slightly larger than that of GaAs.[1-3] This letter reports the first growth of superlattices based on a new alloy system $Zn_{1-x}Mn_xSe$. Because of their wide band gap (~ 2.7 eV at 300 K), these materials may prove useful in the development of blue light emitters and display devices. Also the large exciton binding energies in these materials are of interest both from a basic as well as an applied point of view.

In this letter we report the growth of wide gap semiconductor superlattices of $Zn_{1-x}Mn_xSe$/ZnSe; this is also the first growth of films of the alloy material system $Zn_{1-x}Mn_xSe$ ($0 < x < 0.51$). The various superlattice structures and epilayers have been grown by molecular beam epitaxy. In all superlattices ZnSe was used for the well material with well dimensions ranging from 60 to 90 Å. The $Zn_{1-x}Mn_xSe$ barrier material consisted of various Mn mole fractions ($0.23 < x < 0.51$) with dimensions of 100–150 Å. All superlattice structures consisted of 67 periods grown on a ZnSe buffer layer of 0.57–0.93 μm. In order to characterize the barrier material, ZnMnSe epilayers were grown on a ZnSe buffer layer of 0.25–0.44 μm and were typically 2–3 μm thick. The Mn mole fraction reported here was determined by energy dispersive analysis of x rays (EDAX). The concentrations are believed to be accurate to within 10%. Although $Zn_{1-x}Mn_xSe$ ($0.0 < x < 0.57$) has been grown in bulk crystals, a predominance of the zincblende phase is only observed up to $x = 0.3$, whereas above this mole fraction a predominance of the hexagonal phase exists.[4] For the superlattices and epilayers reported here, only the zincblende phase (100) is present over the entire composition range investigated; no hexagonal phases were observed.[5] The dimensions of the superlattice structure are confirmed by transmission electron microscope (TEM) investigations. Electron diffraction shows satellite spots characteristic of the superlattice structure; bright-field and dark-field imaging reveals the occurrence of very abrupt interfaces between each superlattice layer. Photoluminesence (PL) studies indicate a concave upward bowing of the band-gap variation as a function of Mn concentration. The dominant PL feature of the ZnSe epilayer is a free exciton having a full width at half-maximum (FWHM) of 1.5 meV. The near-band-edge emission for the superlattices shows a continual red shift as the barrier height is increased, dominating the expected blue shift originating from quantum confinement of the carriers. For epilayers of ZnMnSe a broad Mn emission near 2.1 eV becomes dominant as the Mn mole fraction increases, with the near-band-gap luminescence peak becoming less intense. In contrast, the superlattices show virtually no Mn emission for all compositions of the ZnMnSe barrier layers. The PL intensity for the superlattices is 100 times more intense than ZnSe and ZnMnSe thin films at 6.5 K.

The ZnMnSe superlattices and epilayers were grown using a Perkin–Elmer model 400 MBE system. The MBE system and the various *in situ* analytical facilities have been described previously.[6] Briefly however, a movable nude ion gauge is used to measure the individual fluxes and reflection of high-energy electron diffraction (RHEED) is used to observe the growth behavior. The base pressure of the growth chamber is typically 1×10^{-10} Torr.

Three individual effusion cells containing elemental Zn, Se, and Mn were used for sources. These elements were obtained commercially at a purity of 6*N*, 6*N*, and 4*N*, respectively. Each source material was vacuum distilled prior to loading into the MBE system, which provided a final no-

 0003-6951/85/140169-03$01.00

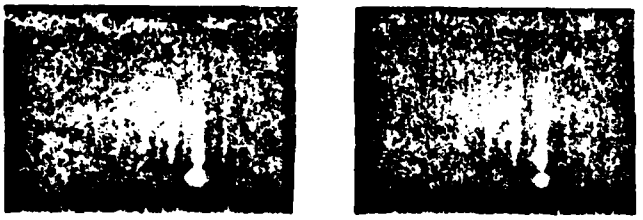

(a) (b)

FIG. 1. RHEED patterns during growth of $Zn_{1-x}Mn_xSe$ ($x = 0.33$)/ZnSe superlattice; (a) ZnSe well layer; (b) $Zn_{1-x}Mn_xSe$ ($x = 0.33$) barrier layer.

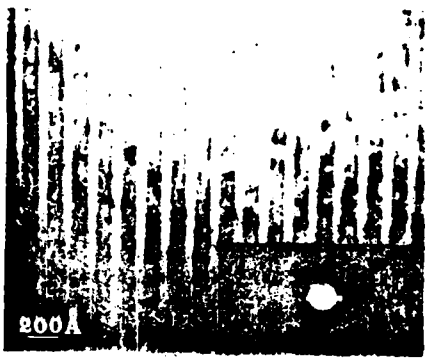

FIG. 2. Dark-field image of the $Zn_{1-x}Mn_xSe$ ($x = 0.33$)/ZnSe superlattice with the (200) diffraction spot (inset) showing satellite spots.

minal purity of 6*N* for the Mn, while also enhancing the purity of the Zn and Se.[7] The temperatures of the Zn and Se ovens were typically 325 and 200 °C, respectively. The Mn oven temperature, however, ranged from 820 to 950 °C to provide for various Mn mole fractions.

GaAs substrates are used for their technological importance and because of the close lattice match with ZnSe (0.25% mismatch). Cr-doped, semi-insulating GaAs (100) substrates oriented 2° off axis were used. The substrates were prepared by standard chemical etching procedures.[6] The substrate temperature was calibrated for each film growth by observing a Au/Ge eutectic phase change. The calibrated substrate temperature for the superlattices and the ZnMnSe epilayers was 400 °C, while growth rates ranged from 2 to 5 Å/s.

Following oxide desorption, the GaAs substrate was monitored with RHEED to observe the initial growth behavior. Since all superlattices and epilayers were grown on a ZnSe buffer layer, the initial growth behavior for ZnSe will be described for a substrate temperature of 400 °C. Immediately after the shutters are opened, the streaked RHEED pattern of the substrate changes to a less intense spot pattern. The presence of the spot pattern suggests that the initial nucleation occurs by a three-dimensional growth mechanism. After approximately one minute, the spots elongate into streaks of uniform intensity. After three minutes a twofold reconstruction pattern appears which remains for the entire period of growth for the ZnSe buffer layer. At the onset of film growth for the ZnMnSe layer (for either the superlattice or the epilayer), the reconstruction streaks become less intense intially, but the intensity increases as the film growth continues. Figure 1(a) shows the RHEED pattern of the ZnSe well layer in a superlattice and Fig. 1(b) shows the ZnMnSe ($x = 0.33$) barrier layer. The high crystalline quality of both ZnSe and ZnMnSe is illustrated by the presence of Kikuchi lines, and very defined, sharp streaks arising from the bulk of the film in addition to intense surface reconstruction streaks. These RHEED patterns persist until the end of the film growth for all superlattices.

Transmission electron microscope observations of cross-sectional specimens were performed with a JEM 200CX electron microscope. These observations have shown that typical dislocation densities in superlattices, buffers, and interfacial regions between buffers and substrates are 10^6, 10^7, and 10^8 cm^{-2}, respectively. Many dislocations which propagate from the interfacial regions are either terminated or reflected by boundaries between superlattices and buffers. A small number of microtwins parallel to {111} planes were also found in the superlattices and buffers. They are often accompanied by dislocations, suggesting that these microtwins provide nucleation sites for the generation of dislocations during film growth. Figure 2 is a dark-field image of a $Zn_{1-x}Mn_xSe$ ($x = 0.23$)/ZnSe superlattice. Shown in the inset of the figure is the (200) diffraction spot which was used for the dark-field image. These films were found to be highly susceptible to the radiation damage induced by the ion beam during sample preparation. Although a very low voltage was used at the final stage of ion thinning, fine structures due to the radiation damage are still seen in the image. From the image, thicknesses of the ZnSe and ZnMnSe layers were estimated to be 63 and 104 Å, respectively. No misfit dislocations are observed at interfaces between superlattice layers as is excepted from the size of the lattice mismatch (0.95%) and the layer thicknesses. The lattice mismatch is totally accommodated by elastic strain giving rise to strained layer superlattices. Both dark-field images and diffraction patterns show the highly regular structure of the superlattice. No sign of disordering at the interfaces is seen in the image. The number of visible satellite spots around the (200) spot is comparable to those of typical AlGaAs-GaAs superlattices. Sixth and seventh order satellite spots are clearly seen in negative films. This suggests that the structural quality of these superlattices is similar to those of well-developed III-V compound superlattices. The greater intensity of the satellite spots at the higher angle side compared to the lower angle side is due to the built-in strain caused by the lattice mismatch.

Photoluminescence measurements were made using UV lines at 3336–3638 Å from a cw argon ion laser. The detection system consisted of a 1/4-m double grating monochrometer in conjunction with a cooled RCA 31034 photomultiplier tube connected to photon counting electronics. Samples were either immersed in LN_2 or suspended in a helium gas at about 6.5 K. The 10-mW beam was focused to a spot 100 μm in diameter.

Photoluminescence measurements were carried out on all epilayers and superlattices at 77 and 6.5 K. Data of band gap versus Mn mole fraction for the epilayers were obtained. The initial variation of the band gap exhibits an upward concave bowing. Such a bowing has also been observed in bulk crystals by Twardowski *et al.*[8] At 6.5 K the ZnSe epilayer (Fig. 3) exhibited a free-exciton dominant peak at 2.799 eV having a full width at half-maximum of 1.5 meV.[7] The two

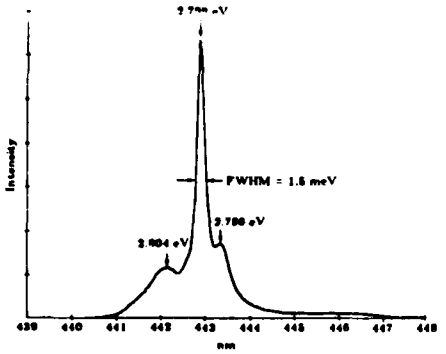

FIG. 3. PL spectrum of the ZnSe epilayer exhibiting the dominant free exciton.

free-exciton features at 2.799 and 2.804 eV are attributed to strain splitting of the valence band[9] (the origin of the strain is the small but finite lattice mismatch between film and substrate). The small feature at 2.796 eV represents an impurity bound exciton. In addition to the near-band-edge emission, a broad deep level emission centered at about 2.4 eV is observed with a peak intensity of 0.02 times the dominant free-exciton feature.

The ZnMnSe epilayers exhibit two peaks which are identified as a near-band-edge emission and a Mn emission corresponding to a Mn^{++} transition. The relative intensities of these two PL peaks vary with Mn mole fraction. As the Mn fraction increases, the PL intensity of the Mn emission increases rapidly with the PL intensity of the band-edge peak decreasing. A broadening of the FWHM is also observed for the band-edge PL peak as the Mn fraction increases, and is attributed to alloy broadening.

When comparing the PL spectra of the superlattices with the various epilayers grown under identical conditions as the material in the barrier, several very interesting differences become apparent. Figure 4 shows a quantitative comparison of a $Zn_{1-x}Mn_xSe$ ($x = 0.33$)/ZnSe superlattice with a $Zn_{1-x}Mn_xSe$ ($x = 0.33$) epilayer mounted on the same header to provide identical conditions of excitation. A typical PL spectrum of the epilayer is obtained exhibiting the dominant Mn emission. In this case the ratio of the intensity of the Mn emission to the intensity of the band-edge emission (R) is 180. In contrast, the superlattice shows an R value of 1.6×10^{-3}. Similar behavior is seen in all the superlattices grown regardless of the barrier height present (i.e., mole fraction of Mn in the barrier layer) indicating significant carrier confinement.

For all samples (again with several samples mounted on the same header) the superlattices were much brighter than the epilayers of ZnSe and ZnMnSe as determined by the relative PL intensities of the band-edge related emission. Specifically, at 6.5 K the PL intensity of the superlattices is 100 times greater than the brightest ZnSe epilayer described earlier. The FWHM of the superlattice ranges from 4 to 9 meV. At 77 K the superlattices show a PL band-edge emission which is 20 times greater than the ZnSe epilayer. For this temperature the FWHM ranges from 8 to 12 meV. All superlattices showed comparable PL intensities when compared to each other.

Although a blue shift might be expected due to quantum

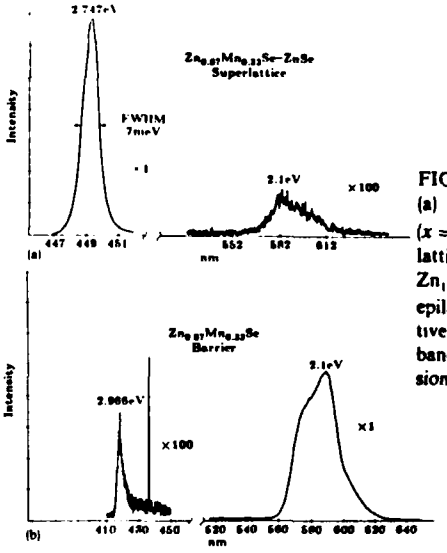

FIG. 4. PL spectra for the (a) $Zn_{1-x}Mn_xSe$ ($x = 0.33$)/ZnSe superlattice and (b) $Zn_{1-x}Mn_xSe$ ($x = 0.33$) epilayer illustrating relative PL intensities of the band edge and Mn emissions.

confinement of the carriers, these wide gap semiconductor superlattices show a continual red shift in energy as the barrier height is increased. Using the Kronig–Penny model with finite barrier height, one predicts a blue shift for the superlattice of 15–22 meV. However, these strained-layer superlattices contain expansive hydrostatic and compressive uniaxial strains which result in a lowering of the conduction-band minimum and a splitting of the valence-band maxima giving rise to the observed red shift. The material system InAsSb described by Osbourn has shown similar behavior.[10] The magnitude of the strain-induced shift can be varied by either changing the Mn mole fraction or the relative thicknesses of the well and barrier. The various superlattices show a red shift from the PL free-exciton energy of the ZnSe epilayer of 3–52 meV.

The authors are very grateful to U. Debska for providing the high-purity vacuum distilled source material, J. K. Furdyna and D. Yoder-Short for many discussions related to bulk ZnMnSe, M. Udo for help in the film growth, and R. Frohne for working through the strain calculations. The authors also thank T. Miller and M. Young for their help in operation of the MBE. L. A. K. would like to thank IBM for fellowship support. This work was supported by Office of Naval Research contract 014-82-K0563, the Air Force Office of Scientific Research grant 83-0237, and NSF-MRL grant DMR-83-16999.

[1]J. P. Faurie, A. Million, and J. Piaquet, Appl. Phys. Lett. 41, 713 (1982).
[2]L. A. Kolodziejski, T. C. Bonsett, R. L. Gunshor, S. Datta, R. B. Bylsma, W. M. Becker, and N. Otsuka, Appl. Phys. Lett. 45, 440 (1984).
[3]R. N. Bicknell, R. W. Yanka, N. C. Giles-Taylor, D. K. Blanks, E. L. Buckland, and J. F. Schetzina, Appl. Phys. Lett. 45, 92 (1984).
[4]D. Yoder-Short and J. Furdyna (private communication).
[5]L. A. Kolodziejski, M. K. Udo, T. C. Bonsett, R. L. Gunshor, S. Datta, R. B. Bylsma, W. M. Becker, and N. Otsuka, paper presented at the General Meeting of the American Physical Society, Baltimore, MD, March 1985.
[6]L. A. Kolodziejski, T. Sakamoto, R. L. Gunshor, and S. Datta, Appl Phys. Lett. 44, 799 (1984).
[7]R. L. Gunshor, N. Otsuka, M. Yamanishi, L. A. Kolodziejski, T. C. Bonsett, R. B. Bylsma, S. Datta, W. M. Becker, and J. Furdyna, presented at the International II-VI Conference, Aussois, France, March 1985.
[8]A. Twardowski, T. Dietl, and M. Demianiuk, Solid State Commun. 48, 845 (1983).
[9]T. Yao, paper presented at the II-VI Internation Conference, Aussois, France, March 1985.
[10]G. C. Osbourn, J. Vac. Sci. Technol. B 2, 176 (1984).

APPENDIX D

Optical properties of ZnSe/(Zn,Mn)Se multiquantum wells

Y. Hefetz, J. Nakahara, and A. V. Nurmikko
Division of Engineering, Brown University, Providence, Rhode Island 02912

L. A. Kolodziejski, R. L. Gunshor, and S. Datta
School of Electrical Engineering, Purdue University, West Lafayette, Indiana 47907

(Received 20 June 1985; accepted for publication 9 August 1985)

Luminescence, excitation, and reflectance spectroscopy have been employed to study the exciton ground state in ZnSe/(Zn,MnSe) multiquantum wells. We find that the ground state shows splittings which are attributed to the superlattice layer strain. The measured large magneto-optical shifts and splittings indicate that the valence-band discontinuity is likely to be quite small in these structures.

The recent successful growth of ZnSe/(Zn,Mn)Se multiquantum wells (MQW) has made another addition to the new family of II–VI compound semiconductor superlattices.[1] The molecular beam epitaxial (MBE) growth of single crystal films of the "semimagnetic semiconductor" (Zn,Mn)Se has also yielded for the first time material which remains in the cubic phase at Mn-ion concentrations in excess of $x = 0.5$, much higher than those in conventionally grown bulk material (where transition to a mixed cubic-hexagonal structure occurs at about $x = 0.1$). The interfacial quality of the ZnSe/(Zn,Mn)Se MQW's is high as evidence by the narrow linewidths observed in the very bright low-temperature photoluminescence and by transmission electron diffraction patterns which show interfacial abruptness form the presence of up to seventh order satellites. In this letter we present results of optical measurements of the exciton ground state in this novel structure, obtained from photoluminescence, excitation, and reflectance spectroscopy at low temperatures. The main early conclusion which emerges from our work is that the valence-band offsets are likely to be very small in this MQW structure and that the exciton states are strongly influenced by the superlattice strains. The presence of the magnetically active ion Mn in the superlattice makes the external magnetic fields particularly useful probes for the spatial extent of the exciton wave function[2] and have provided us with direct evidence for a relatively weakly confined hole state. The results presented below represent a partial summary of work; other details including temperature dependence and lifetime of exciton luminescence will be discussed elsewhere.[3]

The optical studies were carried out on several MQW samples, grown in the [100] direction of GaAs substrates following the initial deposition of a ZnSe buffer layer.[1] The Mn-ion concentrations ranged from $x = 0.23$ to $x = 0.51$. In this letter we show results for a sample with $x = 0.23$, consisting of 67 layer pairs of approximately 67-Å-thick ZnSe wells and 110-Å-thick (Zn,Mn)Se layers. Comparison with optical properties of a (Zn,Mn)Se single crystal film ($x = 0.23$) shows a total band-gap difference of approximately 110 meV for the unstrained heterojunction. Luminescence was excited at 0.325 μm from a low power cw He-Cd laser and collected parallel to the superlattice growth axis (z). Excitation spectra were obtained by using a pulsed dye laser, pumped by an excimer laser source. Standard reflectance measurements were supplemented by differential spectroscopy in which radiation from the He-Cd laser was used to inject a modulating component and the induced incremental changes in reflectance were phase-lock detected. (In such a photomodulation technique exciton-exciton and exciton-free carrier interaction modulated the interband dielectric constant.[4]) The magnetic field experiments were carried out in a superconducting magnet dewar up to $B = 4.0$ T, with the field orientation either parallel or perpendicular to the superlattice z axis and with circular or linear optical polarization.

Figure 1 shows spectral line shape profiles near the exciton ground state for the MQW sample described above, obtained by the different techniques at 2 K. The excitation spectra show the existence of two primary transitions in this spectral region near the exciton ground state (the higher energy resonance had further structure which became particularly evident with the application of an external magnetic field). Somewhat unexpectedly, the amplitudes of the reflectance signals were substantially larger for the higher energy

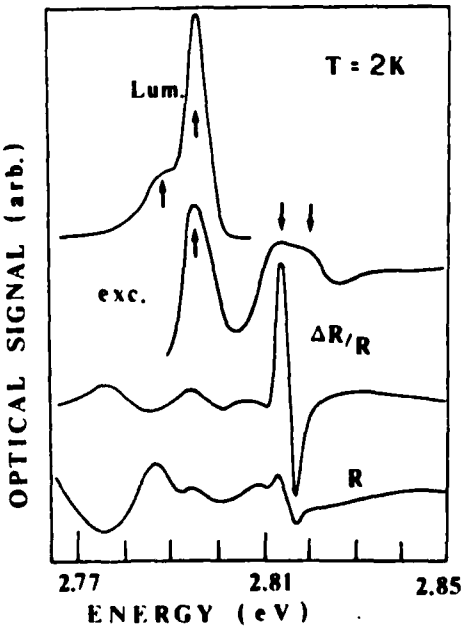

FIG. 1. Illustration of spectral line shapes near the exciton ground state for $ZnSe/Zn_{0.77}Mn_{0.23}Se$ MQW sample of well thickness $L_z = 67$ Å at $T = 2$ K, obtained (from top) by luminescence, excitation (at $\hbar\omega_{exc} = 2.783$ eV), modulated reflectance (low-amplitude resolution), and reflectance spectroscopy. The arrows indicate the primary resonances discussed in text.

 0003-6951/85/210969-03$01.00

components. A weak contribution in luminescence was also seen in this region, becoming relatively larger with increasing temperature.[5] Such a split resonance character in the exciton ground state was observed also in the other MQW samples studied, with the mean separation of energies equal to approximately 19 meV for the case in Fig. 1. More detailed work on the excitation spectroscopy is also being performed by Bylsma and Becker[6] in their study of these superlattice structures. For example, for MQW samples with $x = 0.33$ ($l_w/l_b = 60$ Å/150 Å) and $x = 0.51$ ($l_w/l_b = 90$ Å/130 Å) the corresponding separation was approximately 40 and 50 meV, respectively. The bright low-temperature luminescence peak showed evidence of internal structure, as illustrated by the presence of the distinct low-energy shoulder. The radiative efficiency from all the MQW samples decreased precipitously with increasing temperature, typically showing a reduction by up to two orders in magnitude at 77 K.

The application of an external magnetic field leads to shifts and additional splitting of the exciton ground state in these superlattice structures. These effects originate from the "giant" spin splitting which are due to the spin exchange interaction from the overlap of the exciton wave function with Mn-ion magnetic moments, completely dwarfing the normal Zeeman effects.[7] The results, which combine the use of all of the optical techniques listed above, are partly summarized in Fig. 2, where the main resonances near the exciton ground state are graphed as a function of the magnetic field in the Faraday geometry, and the dominant polarization of the optical signals is labeled. The reflectance spectra (Fig. 1) show the presence of Fabry–Perot fringes; following their subtraction the actual resonances were defined by noting the coincidence with peaks in the excitation spectra. Additional spectral structure was also evident, particularly in the photomodulated reflectance, but we focus our attention here to discuss of the main resonances.

At zero magnetic field ($T = 2$ K) the lowest resonance in Fig. 2 (at about 2.796 eV), measured, e.g., through excitation spectroscopy, was 3–4 meV above the low-energy shoulder of the luminescence. The shoulder grew in amplitude with the magnetic field, becoming the dominant feature at $B = 1.5$ T. Furthermore, a splitting is present at the higher energy resonance and easily seen, e.g., in the excitation spectrum (peaks at 2.810 and 2.816 eV), particularly when extrapolating magnetic field dependent shifts to $B = 0$ T.

We now consider the physical origin of these splittings of the exciton ground state and their behavior in an external field. The appearance of the two main resonances in zero field excitation and reflection spectra of the ground state (and in part their further splitting) is expected from considering the influence of strain on the valence bands in these zinc-blende semiconductors. The rather narrow linewidth (about 5 meV) of the main luminescence peak suggests that such strains are reasonably homogeneous across the MQW structure. Since the lattice constant of (Zn,Mn)Se increases with the Mn concentration x, elastic accommodation of the lattice mismatch in the ZnSe/(Zn,Mn)Se structure (1.05% for $x = 0.23$) implies that the strain in the ZnSe layers has dilational hydrostatic and compressional uniaxial (in z direction)

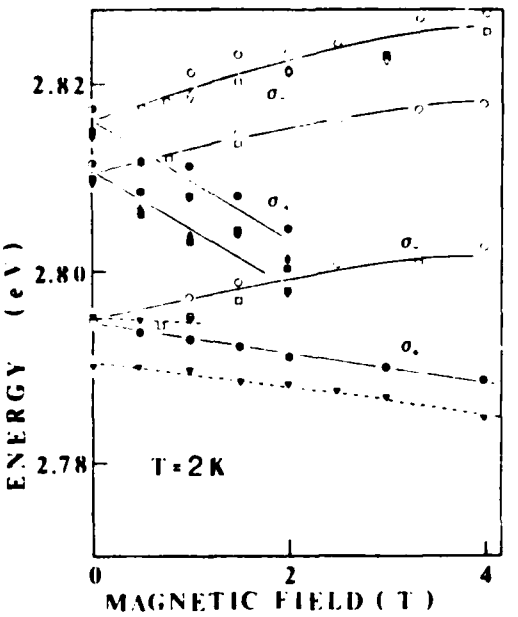

FIG. 2. Summary of data for the split exciton ground state resonance for the $ZnSe/Zn_{0.77}Mn_{0.23}Se$ MQW sample at $T = 2$ K as a function of magnetic field (Faraday geometry). The triangles denote data obtained from luminescence, circles by excitation spectroscopy, squares by reflectance, and diamonds from modulated reflectance. Open and closed symbols refer to opposite signs in the circular polarization as labeled in the figure. The lines are to guide the eye.

components, while the reverse occurs in the (Zn,Mn)Se layers. The uniaxial components split the $|m_j| = 3/2$, $1/2$ hole orbital degeneracy at $k = 0$ so that for the compressive element in ZnSe, the $|m_j| = 1/2$ should push up to higher energy in bulk material while the $|m_j| = 3/2$ state is lowered.[7] Assuming that the elastic constants are equal in both materials, using the available hydrostatic and deformation potential constants for ZnSe, and taking all of the band offset to occur in the conduction band (with $n = 1$ electron confinement energy of about 20 meV), the observed energies and their primary zero field splittings in Fig. 2 (and the trend toward lower photon energies of exciton emission with increasing x in other MQW samples) are in good numerical agreement with estimates.[8] The additional doublet structure in these exciton ground state resonances may also be strain related (e.g., from the strain splitting of the valence band in the (Zn,Mn)Se "barrier" layers, which translated to splittings in the effective quantum well potential). However, the full details of this effect need to take into account proper matching of the wave functions at the interfaces, the effective mass anisotropies, and the (unknown) details of the exciton envelope function.

The magnetic field induced changes in the exciton energy add support to our assignment for strain split valence-band ordering and also yield an idea about the hole confinement in the ZnSe/(Zn,Mn)Se quantum wells. In bulk (Zn,Mn)Se, the spin exchange coefficients α and β for the conduction- and valence-band edges have been measured at low Mn concentrations ($x < 0.10$) and show that $-\beta/\alpha = 4.2$.[9] Assuming that the conduction electron is well confined in the ZnSe layers of the MQW structure and ignoring the exciton influence, we then attribute most of the measured

magneto-optical effects to the valence band. The magnetic field lifts the remaining Kramers degeneracy ($m_j = +3/2, -3/2$ and $+1/2, -1/2$, respectively). The field induced splitting and shifts have contributions through the exchange mechanism from the penetration of the hole wave function into the (Zn,Mn)Se layers. Furthermore, modulation (spin splitting) of the valence-band top of the (Zn,Mn)Se layers by the magnetic field also changes the effective "barrier" height which influences the penetration depth for a confined particle hole. In a self-consistent calculation, these effects need to be included appropriately. The field splitting for the upper resonance in Fig. 2 at a given field is substantially larger than that for the lower resonance. The opposing senses of circular polarization measured for the two transitions are consistent with expected angular momentum selection rules. We also measured the magnetic field induced shifts in low-temperature exciton luminescence in a single crystal film of (Zn,Mn)Se with $x = 0.23$. (In bulk material the luminescence is dominated by the $m_j = -1/2$ to $m_j = -3/2$ conduction- to valence-band transition.) At a field $B = 2$ T, the ratio of the splittings in the MQW sample to that determined from the bulk films is approximately $\Delta E_{qw}/\Delta E_b = 0.18$ and $\Delta E_{qw}/\Delta E_b = 0.41$ for the lower and upper strain split exciton resonances, respectively. From these values we conclude that the assignment of the strain split ordering for the valence band with the $|m_j| = 1/2$ state at the higher energy is correct (the exchange effect being proportional to m_j in bulk semimagnetic material). The two ratios do not differ by the factor of 3 which would occur in bulk (Zn,Mn)Se; this deviation is not surprising considering that the details of the exciton envelope functions for the two transitions are likely to be different. The magnitudes of the observed splittings $\Delta E_{qw}(B)$, however, show directly that a large portion of the hole envelope function resides in the (Zn,Mn)Se layers, implying that the valence-band offset is small. For the $|m_j| = 1/2$ holes state as much as half of the wave function is estimated to reside outside the ZnSe layers if we assume an infinite Mn-concentration gradient (i.e., no diffusion to the ZnSe layers). When rotating the magnetic field to direction perpendicular to the superlattice axis (z), we have seen only small changes in $\Delta E_{qw}(B)$. This is in contrast with behavior observed in the CdTe/(Cd,Mn)Te MQW's[2] and suggests that the hole (and the exciton) in the ZnSe/(Zn,Mn)Se system are relatively three-dimensional for the 67-Å well width in the case considered here (bulk exciton Bohr radius in ZnSe is approximately 28 Å).

While these results need to be better correlated with more precise calculations, we estimate from the magnetic field studies that the average valence-band offset in the ZnSe/(Zn,Mn)Se quantum wells is likely to be less than some 20 meV. As shown above, the strain splittings of the valence-band top are of comparable magnitude for the sample discussed here and increase for structures with higher Mn-ion concentrations in the "barriers." This may affect significantly the degree of confinement for the "heavy" and "light" holes; in principle it would be possible for one of them to be in confined particle states and the other in the (delocalized) continuum. We particularly note the puzzle concerning the relative amplitudes of the excitation and reflectance spectra in Fig. 1, where the reflectance amplitudes are much larger for the upper strain split resonance; this behavior could be related to such differences in the valence-band potentials. Generally, for weak confinement of the holes the exciton problem becomes considerably more complicated than that allowed for by presently available calculations [constructed mainly for the GaAs/(Ga,Al)As quantum well case]. At the same time, it is unlikely that the ZnSe/(Zn,Mn)Se quantum well system is significantly of type II since the magnitudes of the observed magneto-optical shifts are not large enough to support this conclusion. Other complications arise from the strain induced anisotropies which lead to anomalous effective mass changes at the heterointerfaces and which might considerably modify the spatial extent of the exciton wave function (possibly enhancing its amplitude near the interfaces).

We wish to thank J. Torreao for expert help in these experiments. The work at Brown University was supported by the Office of Naval Research contract N00014-83-K0638 and a Department of Energy grant DE-FG02-84-ER13235. The work at Purdue University was supported by the Office of Navel Research contract N00014-82-K0563, the Air Force Office of Scientific Research grant 83-0237, and NSF-MRL grant DMR-83-16988. L. A. K. would like to thank IBM for fellowship support.

[1] L. A. Kolodziejski, R. L. Gunshor, T. C. Bonsett, R. Venkatasubramanian, S. Datta, R. B. Bylsma, W. M. Becker, and N. Otsuka, Appl. Phys. Lett. 47, 169 (1985).
[2] X.-C. Zhang, S.-K. Chang, A. V. Nurmikko, L. A. Kolodziejski, R. L. Gunshor, and S. Datta, Phys. Rev. B 31, 4056 (1985).
[3] X.-C. Zhang, Y. Hefetz, S.-K. Chang, J. Nakahara, A. V. Nurmikko, L. A. Kolodziejski, and R. L. Gunshor, Proceedings of Conference of Modulated Semiconductor Structures, Kyoto, Japan 1985 (to be published).
[4] Y. Hefetz, X.-C. Zhang, and A. V. Nurmikko, Phys. Rev. B 31, 5371 (1985).
[5] Data also corroborated by measurements by T. C. Bonsett and R. B. Bylsma (private communication).
[6] R. B. Bylsma and W. M. Becker (unpublished).
[7] See, e.g., F. H. Pollak and M. Cardona, Phys. Rev. 172, 816 (1968).
[8] R. Frohne and S. Datta (unpublished).
[9] A. Twardowski, T. Dietl, and M. Demianuk, Solid State Commun. 48, 845 (1983); D. Heiman, Y. Shapira, and S. Foner, Solid State Commun. 51, 603 (1984).

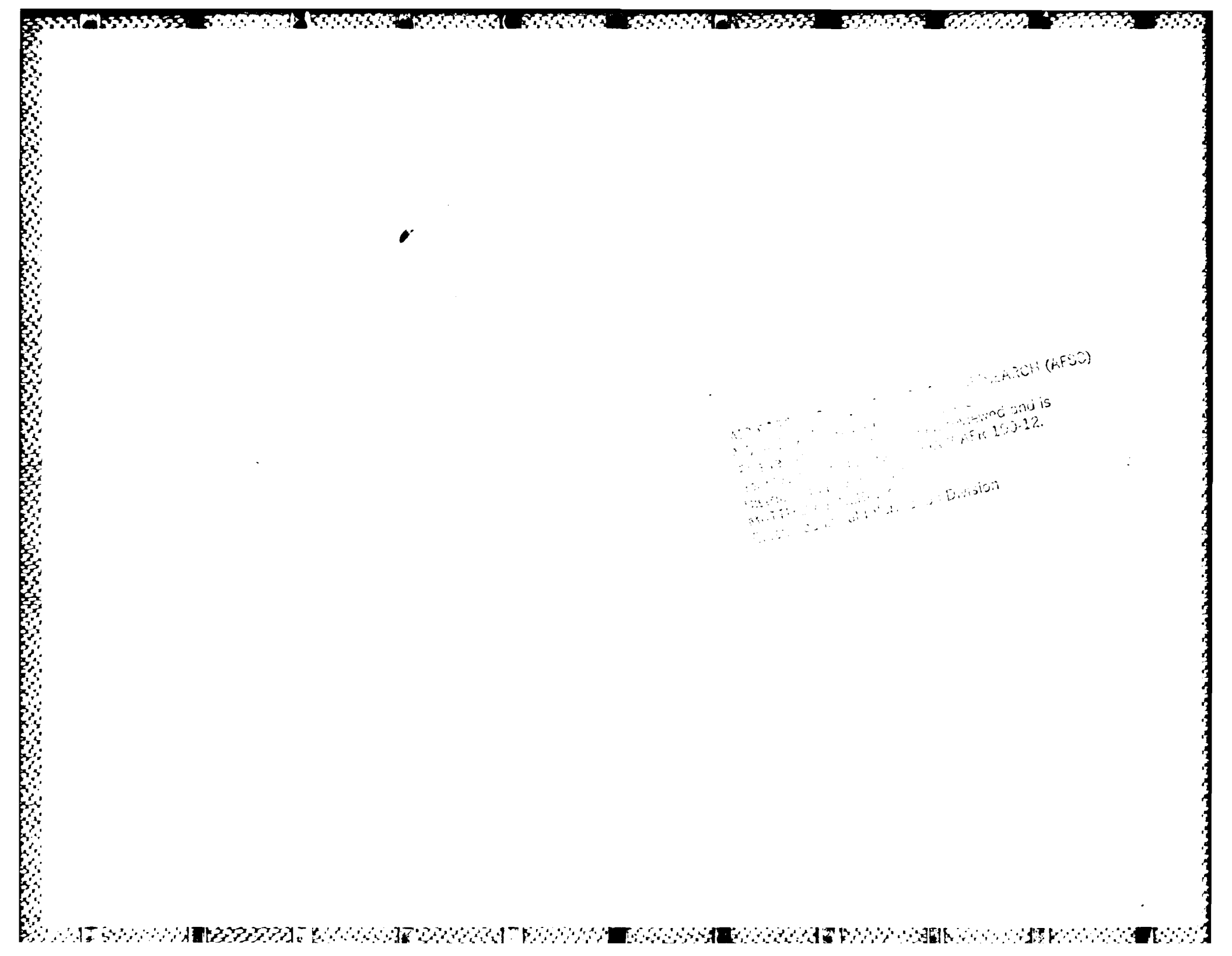
SEARCH (AFSC)
AFR 190-12.
Division

END

5-87

DTIC